Geochemical and palaeomagnetic characteristics of a Swedish Holocene sediment sequence from Lake Storsjön, Jämtland

Joakim Robygd

Dissertations in Geology at Lund University,
Master's thesis, no 424
(45 hp/ECTS credits)

Department of Geology
Lund University
2015

Geochemical and palaeomagnetic characteristics of a Swedish Holocene sediment sequence from Lake Storsjön, Jämtland

Master's thesis
Joakim Robygd

Department of Geology
Lund University
2015

Contents

Cover Picture: Fieldwork at Lake Storsjön sketch. Photo: Joakim Robygd

Abstract

JOAKIM ROBYGD

Robygd, J., 2015: Geochemical and palaeomagnetic characteristics of a Swedish Holocene sediment sequence from Lake Storsjön, Jämtland. *Dissertations in Geology at Lund University*, No. 424, 33 pp. 45 hp (45 ECTS credits).

Abstract: As a part of a French-Swedish collaboration project to reconstruct middle to northern European climate variations during the Holocene, a sediment sequence from Lake Storsjön, Jämtland was retrieved and analysed for geochemical and palaeomagnetic properties. The subsampled sequence, composed of one freeze core and three Niederreiter piston cores, revealed information of both climatic, environmental and anthropogenic changes over the past 10,800 years. As previously theorized by several Swedish authors, Lake Storsjön likely was covered by a complex of shifting ice-lakes before the modern lake was isolated. This study reveals the timing of the ice-lake drainage to have occurred at around 9629 cal yrs BP, portrayed as a lithostratigraphic change from laminated clays to a more organic rich clay gyttja deposit. As a response to increasing organic production in the newly isolated lake, hypoxic to anoxic conditions arose, seen in the elemental proxies of Mo/Al and Mn/Fe ratios, and resulted in sulphide reducing bacteria forming authigenic greigite of which fossil magnetosomes are recorded by the mineral magnetic assemblage. A similar situation arose when a likely more persistent ice cover during the 8.2 kyr event induced low oxygen conditions, again inducing authigenic greigite formation. The whole post-drainage interval of the sediment sequence is banded by black layering which is interpreted as paramagnetic pyritization of magnetotactic bacterial magnetite induced by low oxygen and reducing conditions, in turn caused by certain events of strong spring meltwater pulses. The black banding is inferred as being composed of a relatively coarser grain size by the elemental ratio of Zr/K which would be explained by the generally increased catchment overflow during such events. In the more recent parts of the sequence, socioeconomic crises derived from disease (Black Death) as well as climate change (Little Ace Age) are visible as a change in land use. The timing of the LIA in the area is interpreted as has been most severe during a 60 yr period between 330-270 cal yrs BP. With the onset of the industrial revolution, metal pollution has followed. Elemental concentrations of Pb, Cu, Zn and As have risen steadily over the past 130 cal yrs BP. Calculated anthropogenic Pb exhibits concentration peaks corresponding well with the long range transported Pb peaks at AD 1200, AD 1530 and AD 1975 with reference datasets from both south and north of Lake Storsjön. A large change in the physical and chemical records of Lake Storsjön is also found in the sediments deposited during the past 70 yrs as a response to the lake being used as a hydropower production reservoir. The latter however, needs to be more thoroughly examined to properly resolve the ongoing change.

The sediments of Lake Storsjön were dated with both relative (palaeomagnetic secular variations, pollution Pb) and absolute (^{14}C, ^{137}Cs) dating techniques. The resulting age model was a mixture of the both. The age model relied heavily on the relative dating with palaeomagnetic secular variations (PSV) but was in good agreement with inserted absolutely dated material. The carriers of the natural remanent magnetisation (NRM) are interpreted as relying heavily on bacterial magnetite and have a very stable NRM throughout the sequence as inferred from its maximum angular deviation (MAD). Declination events proved more useful in constructing the early part of the age model while inclination events were used to construct the older parts. Sedimentation rates were invariable during long term climatic stability and generally increased with enhanced human activities.

Keywords: Jämtland, geochemistry, palaeomagnetism, PSV, sedimentation rate, Holocene development, geochronology, climate change

Supervisor: Dan Hammarlund

Subject: Quaternary Geology

Joakim Robygd, Department of Geology, Lund University, Sölvegatan 12, SE-223 62 Lund, Sweden. E-mail: j.robygd@gmail.com

Svensk sammanfattning

JOAKIM ROBYGD

Robygd, J., 2015: Geochemical and palaeomagnetic characteristics of a Swedish Holocene sediment sequence from Lake Storsjön, Jämtland.. *Examensarbeten i geologi vid Lunds universitet*, Nr. 424, 33 sid. 45 hp.

Sammanfattning: Som en del i ett fransk-svensk sammarbete i syfte att rekonstruera holocena klimatförändringar i centrala och norra Europa, togs en sedimentsekvens upp från Storsjön, Jämtland och analyserades för geokemiska och paleomagnetiska egenskaper. Den provtagna delen av sekvensen, bestående av en fryskärna samt tre Niederreiter-kärnor, tydliggjorde förändringar orsakade av klimat samt antropogen påverkan de senaste 10800 åren. Det har tidigare spekulerats i att Storsjön efter deglaciationen var täckt av en serie issjöar innan den moderna sjöbassängen etablerades. Den här studien avslöjar att det sista issjö-stadiet avslutades omkring 9629 år före nutid. Tappningen av issjö-stadiet är synligt i sedimentsekvensen som en litostratigrafisk förändring från laminerade leror till en mer organisk lerig gyttja avsättning. I respons till sagd förändring uppstod hypoxiska till anoxiska förhållanden, återspeglat i de geokemiska elementar-kvoterna Mo/Al och Mn/Fe. De låga syreförhållandena gav upphov till sulfidreducerande bakteriell nedbrytning av organiskt material och gynnade formationen av autogen greigit av magnetotaktiska bakterier. Dessa fossila magnetosomer reflekteras tydligt i den mineralmagnetiska sammansättningen samt i koncentrationen av svavel. En liknande situation uppstod då förmodade förlängda istäcken minskade syretillgången i bottenvattnet under den så kallade 8.2 kiloanno händelsen där årsmedeltemperaturen sänktes avsevärt under en period. Under denna period tolkas den magnetiska sammansättningen åter att bestå av autogen greigit från magnetotaktiska bakterier. Under hela perioden av lerig gyttja avsättning så är svarta band utspridda genom sediment sekvensen. Dessa band tolkas som pyritisation av magnetotaktisk magnetit som uppstått i respons till kortare intervall av minskad syretillförsel. Anledningen till det minskade syret tros vara episoder av intensifierad snösmältning och avrinning. Denna tolkning stöds vidare av en härleden ökad minerogen kornstorlekssammansättning av de svarta banden från elementarkvoten av Zr/K. I den senare delen av sekvensen är socioekonomiska kriser härrörande från sjukdom (Digerdöden) samt klimatförändring (lilla istiden) synliga som härledda förändringar i markanvändning i avrinningsområdet. Lilla istiden är bedömd att ha varit mest förödande för jordbruket mellan 330-270 år före nutid. Den industriella revolutionen har bevisligen medfört föroreningar av tungmetaller. Koncentrationer av Pb, Cu, Zn och As har stigit kontinuerligt över de senaste 130 åren. Beräknat föroreningsbly sammanfaller väl med koncentrationstoppar av långtransporterade blyföroreningar vid år 1200, 1500 och 1975 från referensdataset både söder och norr om undersökningsområdet. En stor förändring i de geokemiska och paleomagnetiska egenskaperna syns under de senaste 70 åren som en respons till utbyggnationen av en kraftverksdam men kommer kräva en mer detaljerad studie för att utröna exakta konsekvenser av de förändrade förhållandena.

Sedimenten daterades med både relativa (paleomagnetiska sekulära variationer, föroreningsbly) samt absoluta (^{14}C, ^{137}CS) dateringsmetoder. Den slutgiltiga åldermodellen bestod av en kombination av de båda. Åldersmodellen är till stor del uppbyggd av PSV datering men insatta absoluta datum passade väl in i det interpolerade relativa dateringarna. Bärarna av NRM tolkas bestå till stor del av bakteriell magnetit och har en väldigt stabil NRM signal genom hela sekvensen härledet från de låga MAD-värdena. Deklination användes först och främst till uppbyggnaden av den senare delen av åldersmodellen och inklination till den tidigare delen. Sedimentationshastigheter visade låg variation under härledd klimatisk stabilitet och ökade generellt med ökad mänsklig aktivitet i området.

Nyckelord: Jämtland, geokemi, paleomagnetism, PSV, sedimentationshastighet, Holocen utveckling, klimatförändringar, geokronologi

Joakim Robygd, Geologiska institutionen, Lunds Universitet, Sölvegatan 12, 223 62 Lund, Sverige. E-post: j.robygd@gmail.com

1 Introduction

During the past few decades, anthropogenic climate and environmental change has been broadly accepted and subject for intense discussion and research. When confronted with the matter of present day and future change in climate, the geological society often seeks to investigate the past to be able to quantify and identify cause and effect of such changes. Put in the words of James Hutton (1726-1797), "*The present is the key to the past*", this reasoning also applies in the opposite temporal direction.

To acquire knowledge about spatial and temporal changes in environmental settings, natural archives such as lake sediments, have been and still are, a valuable tool (Cohen 2003 & Smol 2008). A good spatial cover of such information is crucial for understanding of large scale climate variability which in turn is linked to the catchment scale responses in terms of biotic and abiotic changes in the lake sediments, which are ultimately examined. However, the driving factors behind catchment scale changes need to be identified as regional/national/global or purely local through spatial cross validation to be able to contribute to the overall task (Dalton et al. 2005).

The bearers of the information contained in a sediment sequence are numerous and include both biotic and abiotic proxies (Engstrom et al. 1985, von Grafenstein et al. 1999, Davis et al. 2003, Petterson et al. 2010), however, it is a question of expertise and/or availability that decide which proxy or proxies that are best suited for the question at hand. Battarbee et al., 2002 compared multi-proxy data with monitoring data from seven European mountain lakes over the past two centuries and found a generally weak correlation. The study highlights two major issues when dealing with proxy-based climatic or environmental lake sediment studies. One; the problem of inaccurate dating discrediting a perfectly fine data set by placing events in an untimely order and, two; the need for cross validation between proxies. The study also suggests that proxy based studies generally capture changes on a relatively coarse temporal resolution.

This thesis is part of a large scale multi-proxy reconstruction of Holocene central and northern European climate. The thesis is aiming to set an initial reference age scale of indices of climatic and anthropogenic change in the area to be complemented by further quantitative oxygen isotope studies from lake sediments and speleothems from nearby records.

In this thesis, a multi-proxy approach is applied to qualitatively reconstruct the postglacial development of a northern Swedish lake (Lake Storsjön) previously dammed by an ice-lake and now a regulated reservoir for hydropower production. A variety of dating techniques are applied to ascertain precise geochronology and to test the accuracy and cross validity of the dating tools.

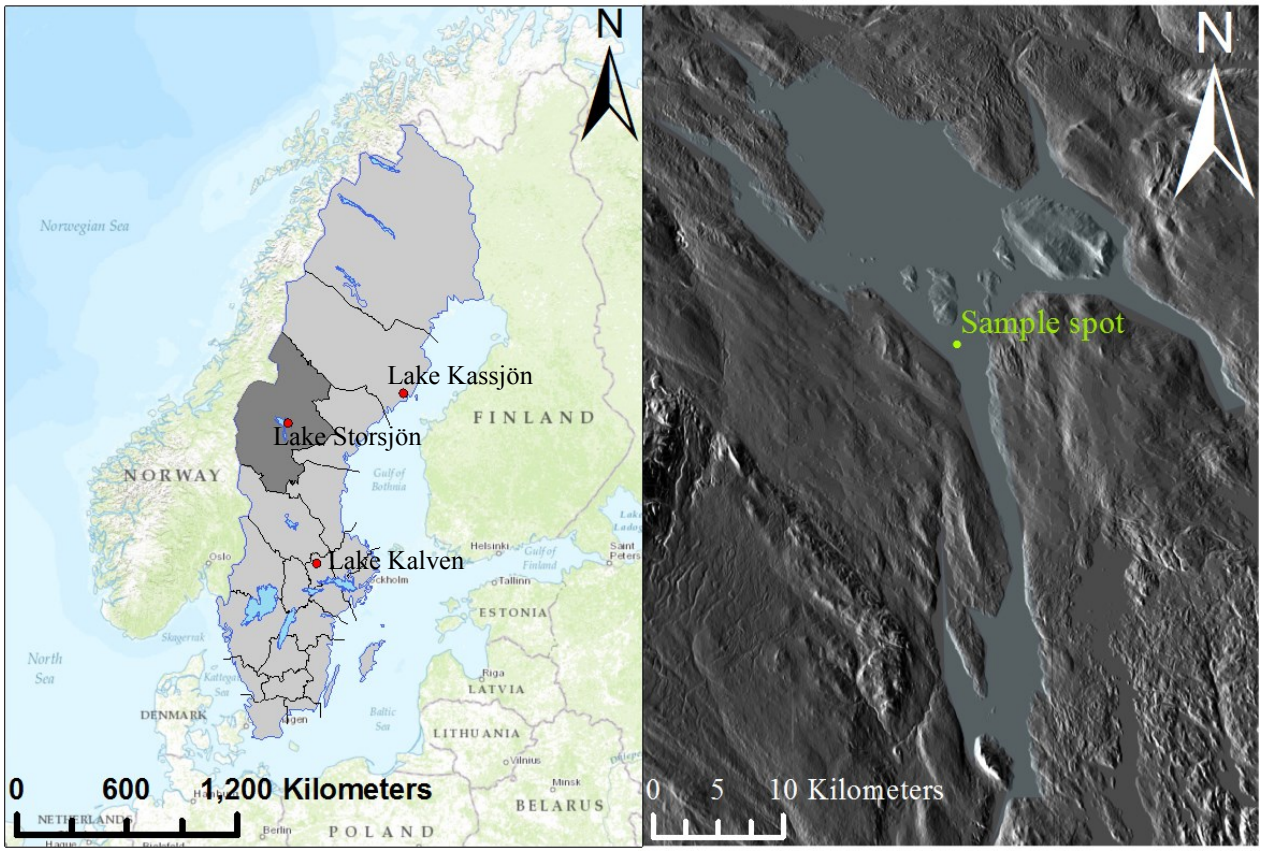

Figure 1. Overview map of Lakes Storsjön's location in Scandinavia and elevation LiDAR with denoted sampling site. Red dots represent lakes from where pollution Pb data is presented.

1.1 Study area

Lake Storsjön, situated in Jämtland, Sweden (Fig. 1) is with its 464 km^2 and ~1000 km^2 catchment area, the fifth largest lake in Sweden and is since 1938 regulated for hydroelectric production. The lake is oligotrophic and has a mean depth of 17 m (Axenrot et al. 2013). The bedrock surroundings (Fig. 2A) are composed of mainly greywackes, shales and limestone of Caledonian orogeny covered by diamicton and clayey diamicton (Fig. 2B) (Lundqvist 2009). The surrounding vegetation is dominated by mires and coniferous forest although the clay rich soil and carbonate bedrock have allowed for a certain degree of cultivation of the lands. Urban influence is minor, although Östersund with its ~40000 inhabitants is situated at the east-central shore of the lake.

Lake Storsjön was deglaciated at approximately 10000 cal yrs BP (Lundqvist 2009), but evidence of stagnated ice in the area after deglaciation are numerous. South of Lake Storsjön, on the sides of the mountain complex of Oviksfjällen and Västerfjället, evidence of shore lines and terraces associated with an ice dammed lake can be found (Lundqvist 1973, Borgström 1989). The valley below these shorelines also contains typical glacial clays (Lundqvist 1973).

The site chosen for sediment retrieval is a 33 m deep basin located in between the island of Norderön and the village of Vällviken (N 6998974, E 468373). No major inlets are found in the vicinity of the coring site. The sediment depth was estimated to be around 9 m on the basis of an seismic survey performed in November 2013.

1.2 Dating techniques

Since a vast number of different techniques have been developed to, more or less, precisely determine the age of various sediments at certain depths, the law of superposition still acts as a control of the absolute dating techniques. If not apparently disturbed, one can safely assume that sediments have accumulated up-

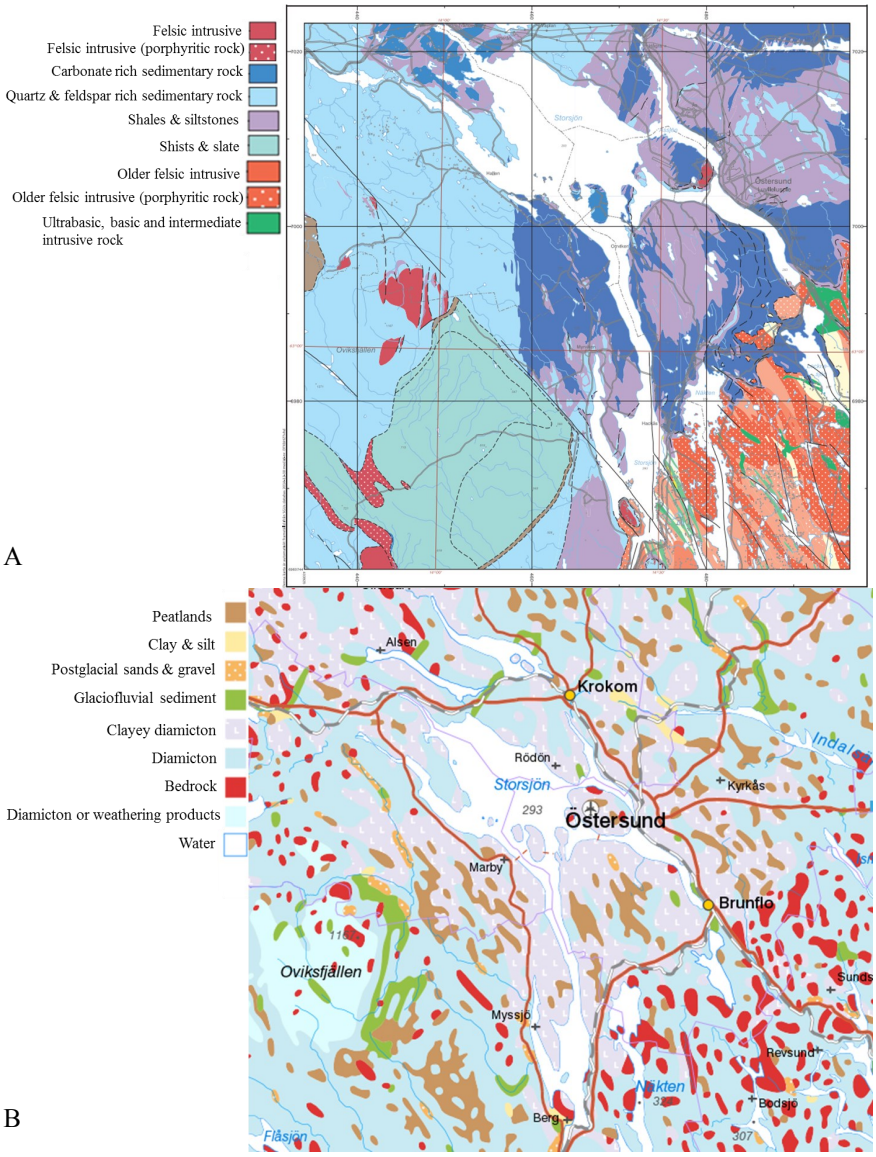

Figure 2. Bedrock (A) and soil cover (B) maps over the surrounding areas of Lake Storsjön

wards, i.e. formation of younger sediments as the sediment sequence builds up. However, constraint on the timing of an event and its errors is an invaluable tool in all geological work, hence it has been given considerable attention. The methods used for dating of the lake sediments described in this thesis are summarized below.

1.2.1 Lead pollution history

X-ray fluorescence (XRF) is a useful tool to rapidly identify elemental concentrations of a sediment sample (Boyle 1998). Applied to lake sediments and palaeolimnology, XRF can be applied to discrete samples or scanned over a whole core, thus displaying downcore changes in elemental composition. The method, however, is generally not sensitive enough to identify isotopes of the elements.

One element is of special interest when it comes to geochronology, namely lead (Pb). Lead concentrations and isotopic ratios have been applied successfully as age constraints in age models by several authors (Renberg et al. 1994, Brännvall et al. 2001, Bindler et al. 2009, Weiss et al. 1999). The isotopic ratio $^{206}Pb/^{207}Pb$ changes depending on the Pb origin, and these changes have been coupled emission sources through history. The most prominent changes occur around 0 AD, coupled to the Greek-Roman mining activities. Around 1200 AD and 1530 AD changes in the isotopic ratio originates from intensified metallurgy in Europe and a very recent change occurs at AD 1975 when leaded petrol use was at its prime (Renberg et al. 1994). These isotopic changes can also be seen as prominent increases in total Pb concentration corresponding to the same dates.

1.2.2 Radiocarbon

The constant bombardment of cosmic radiation in the upper atmosphere causes ^{14}N to capture a neutron and emit a proton, hence forming the radioisotope ^{14}C ($t/_2$: 5730yr). Once the ^{14}C oxidizes to $^{14}CO_2$ it readily incorporates into plant tissue. The plant lives out its days, being roughly in ^{14}C equilibrium with the atmosphere, since new radiocarbon is constantly formed as radiocarbon decays within the plant. When the plant dies the "radiocarbon clock" starts since no more ^{14}C can replenish what is lost by decay (Bowman 1990). Under optimal conditions terrestrial plant material is immediately transported to a lake where it rapidly sinks down and becomes incorporated in the sediments. Several thousands of years later, this would allow one to identify the macrofossil and translate the amount of remaining ^{14}C to $^{13}C+^{12}C$ ratio into an age, assuming that initial conditions were the same as today (Oswald et al. 2003). However, this is not the case, the atmosphere has been diluted with "dead" carbon originating from ^{14}C depleted fossil fuel. The convention is to compare the measured amount to the ^{14}C levels of 1850 (i.e. before the industrial revolution) and the "zero-age" is set to 1950 (Bowman 1990).

1.2.3 ^{210}Pb and ^{137}Cs

As the radiocarbon method has its limitations of not reliably dating more recent sediments, other methods must be used to date the uppermost sediments. In the ^{238}U decay series, an intermediate isotope, ^{226}Ra eventually decays into gaseous ^{222}Rn which escapes into the atmosphere. The rather short lived ^{222}Rn ($t/_2$: 3,8 days) decays in the atmosphere to form ^{210}Pb ($t/_2$: 22,3yr) which is quickly removed from the atmosphere via precipitation (Fig. 3). The newly formed ^{210}Pb decays through a series of very short-lived isotopes into stable ^{206}Pb. However, the sediments also contain a background value of ^{210}Pb which must be measured to be able to distinguish between the two sources. Once the ^{226}Ra-^{210}Pb equilibrium has been measured the remaining fraction of ^{210}Pb (so called unsupported fraction) can be measured (Appleby 2001).

The disintegrations ^{210}Bi to ^{210}Po, which are intermediate radioisotopes, are counted by gamma emission which renders the material unharmed. This allows for further analysis of other radioisotopes in the sample such as ^{137}Cs. ^{137}Cs was intensively spread across the globe during the nuclear bomb tests during the 1950-60's with its peak in 1963. The isotope was later enriched in northern Europe in 1986 when the nuclear power plant in Chernobyl malfunctioned and exploded. These two massive peaks in artificial ^{137}Cs now serve as excellent chronomarkers (Cohen 2003 & Smol 2008).

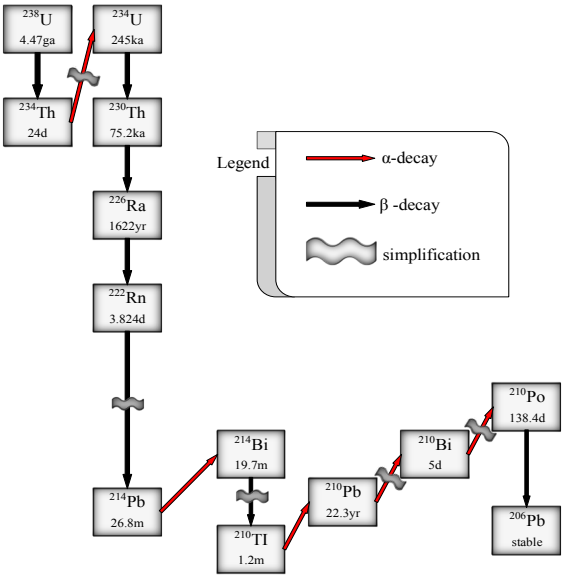

Figure 3. ^{238}U decay chain down to stable ^{106}Pb.

1.2.4 Palaeomagnetic secular variations

Paleomagnestism comprises many applications of the magnetic characteristics of sediments. However, in the purposes of dating one should pay extra attention to the measurement of natural magnetic remanence (NMR). As to be expected by a dynamic system such as our planet, no natural phenomena remain constant through time. The geomagnetic fields' variations in strength and polarity have fortunately been recorded

by various natural archives, such as lava beds and lake sediments. The position of the north geomagnetic pole (NGP), the vertical vector and the intensity of the geomagnetic field at the time of burial are recorded by sedimentary magnetic mineral grains as they get locked in position by the overburden. The angle of the recorded NGP relative to the true north is called declination (D) and the vertical vector of the geomagnetic field is called inclination (I) (Thompson & Oldfield 1986). By measuring the variations of D, I and geomagnetic intensity, palaeomagnetic secular variations (PSV) can be obtained. PSV of I and D are considered to have varied in the same fashion through time for specific regions. For example, Snowball et al. (2007) made use of such secular variations to create a stacked master curve of I and D, respectively, from independently dated lake sediment cores in Scandinavia called FENNOSTACK for inclination and declination and FENNORPRIS for palaeointensity. Nilsson et al. (2014) also constructed a model in which PSV data can be modeled to reflect the conditions at a specific location using PSV data from a geographically constrained area and adjust them to fit the predictions of geomagnetic dipole (GDP) movements in the selected area. Available model adjusted data using this model for the location of Lake Storsjön archaeomagnetic PSV model (ARCH3k) from Korte et al. (2009) and the palaeomagnetic PSV model (pfm9k.1A) from Nilsson et al. (2014). The master curves from FENNOSTACK and FENNORPIS together with the modeled data from Nilsson et al. (2014) and Korte et al. (2009) can be used to indirectly date Scandinavian lake sediments through ”wiggle matching” between PSV records (eg. Stanton et al 2010).

1.3 Age depth model

When performing accelerator mass spectrometry (AMS) radiocarbon analysis, a ^{14}C age of the sediment is obtained. However, the derived date does not reflect the true age of the sediments. Instead the date simply reflects the residual ^{14}C activity compared to a modern standard. To be able to convert a radiocarbon age to a “real” age, an external control is needed. This is achieved by comparison with a calibration curve, which comprises the relationship between radiocarbon age and calendar age of several independently dated treering series (Reimer et al. 2013). The calibration curve is however not smooth and one ^{14}C age probability distribution might fit equally well in one, two or several places on the calibration curve. Fortunately, one seldom dates only one sample of a lake sediment sequence. By dating at several depths downcore, the many radiocarbon ages can be wiggle matched for the best fit on the calibration curve.

Constructing age models without the aid of radiocarbon dating can be achieved by combining inferred relative dates through the above mention techniques. Doing so, the task at hand becomes trying to piece together dates derived from different techniques (i.e. ^{210}Pb, PSV, pollution Pb etc.) with variable and sometimes arbitrary errors.

The problem which arises is that not every single centimeter can be dated through a several meters long sequence due to the timely and sometimes costly nature of the analyses. Therefore, the logical way to proceed is to estimate the age of the sediments between the dated sections (i.e interpolation); this can be achieved in many ways. Simple linear point to point interpolation neglects one of the basic controls of the age variance of the sediment sequence, namely sedimentation rate. When drawing a straight line between points one has to assume that sedimentation rates are changing at this very point in time. This could of course in some cases be visually confirmed or rejected judging from stratigraphical changes in the sediments.

More sophisticated methods exist to estimate the ages between several points, taking into account the mean sedimentation rate as well as stratigraphical changes, in a much generalized way. The method of probability based on previous information is called Bayesian statistics and is used by many of the popular calibration softwares of today (Bchron, oxcal etc.). In this paper however, the program of choice is the Bacon 2.2 R module (Blauw & Christen 2011) which make use of the “prior knowledge” of sedimentation rates. The program allows the user to adjust the prior setting such as estimates of the sedimentation rate and rate of change. The program also suggests the prior settings if the estimation does not add up to the interpolated changes. Through the fully automatic markov chain monte carlo (MCMC) algorithm “twalk” (Christen & Fox 2010), the program calculates the optimal position of each interpolated point, which resolution is set as one of the priors, through millions of iterations.

2 Material and methods

2.1 Field work

Coring sites were selected on the basis of a seismic survey conducted in November 2013 where sufficient sediment thickness and undisturbed bottoms were found.

During seven days in early April, 2014 two sediment sequences from Lake Storsjön were retrieved from the ice, one of which is discussed below. Surface samples were obtained using a freeze corer (Renberg & Hansson 2010). At greater sediment depth a hammer-driven Niederreiter piston corer fitted with an 86 mm diameter PVC tube was used to collect two meter long cores, each with one meter overlap. The piston coring system was a modified version using only two winches, excluding the use of the hammer-cable. However, in loose surficial sediments, the old system approach was used where the hammer rod is in a fixed position to prevent tilting of the device. Overlapping sections were obtained from an adjacent hole in the ice, approximately two meters away. All surface sam-

ples were obtained initially at greater distance (~4 m) from the piston coring site to avoid contamination of surface sediments.

The 2-m sequences were sealed with floral foam and taped caps in both ends and surface direction was noted on the PVC tube. The freeze core was cleaned off from excess sediment and the steel wedge was removed, leaving only frozen sediments and ice. The hollow sediment/ice wedge was wrapped in plastic bags and transported to a local freezer facility for storage before transportation to the laboratory.

2.2 Subsampling

The freeze core samples were stored at a constant temperature of -22°C in the Department of Chemistry at the Faculty of Engineering, Lund University during all subsampling. The sediment was cut with a handsaw, removing one of the broad sides of the wedge. The resulting "sediment plank" was planed down with a woodworkers' plane in the direction of the natural bedding to remove any cross-level contamination (Fig. 4). The planed planks were subdivided into 10 cm pieces for easy handling during subsampling. The top ten centimeters were cut with a band saw in 1 cm intervals from bottom towards the top. The topmost sediments were kept larger due to differences in density and compaction.

The following subsections were also sampled in the resolution of 1 cm, yielding sediment slabs of approximately eight millimeters. The subsection 10-20 cm in the freeze core were cut in a 0,5 cm resolution. After thawing the sediments were transferred into plastic cubes (7cm^3) and stored cold (4ºC) prior to analysis.

The piston cores were stored cold (4°C) until opening. A wooden box in two parts was constructed to centre and expose the diametrical sides of the tube. The cores were cut along the edges, only cutting through the tube. The sediments were cut using a piano wire which was dragged through the side-openings of the tube. One half was subjected to sampling while the other half serves as a reference.

The sediments were thoroughly examined, described, measured and photographed before any subsampling started. In order to assure an as complete stratigraphic series as possible the overlapping sections were put in to a common depth scale. This was accomplished by identifying stratigraphic tie-points on each corresponding overlap to create a composite depth scale for the sequence. Where the sections were homogenous or without clear stratigraphic markers, half the length of the section was correlated with the middle of the overlapping sequence. This, however, only occurred in deep cores without any clear stratigraphy.

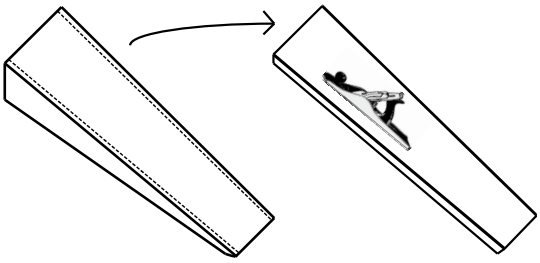

Figure 4. Graphical illustration of freeze core preparations.

Samples for ^{14}C dating (macrofossils) were picked by hand, rinsed and identified under a microscope prior to analysis. At one certain, presumed important level (3.197-3.227 m) low in protruding macrofossils, a bulk sediment sample was sieved through a 125 µm metal mesh to recover macrofossil material for dating.

The sediments were later scraped clean and 7 cm^3 cubes for subsequent palaeomagnetic measurements were pushed into the sediments at three centimeter intervals (starting at 1.5 cm). Subsequently, the sediments were extruded from their plastic liners and cut into 1 cm slices, cutting carefully around the cubes. The cubes were capped and stored humid and cold until later analysis. This procedure was carried out on the upper 3.99 meters of the sequence.

2.3 Laboratory work

2.3.1 Loss-on-ignition

Samples were transferred into numbered and preweighed crucibles and then weighed again. The samples were then combusted in a furnace oven at 550º for four hours. The recommendations for the procedure outlined by Heiri et al. (2001) were applied when possible. Especially for the upper parts of the freeze core, where sample size was small, sidesteps from these recommendations had to be made.

2.3.2 X-ray fluorescence

Dry sediments were transferred and gently packed in temporary containers with a plastic film exposing the sediments to the sensor of a Thermo Scientific Niton XL3t Goldd+ XRF analyzer. The analysis was carried out in mining mode (Cu/Zn) and the high range was excluded for faster handling of the procedure. All measurements were conducted in duplicates and the analytical error of major elements ranged from 0.48% to 5.2% and between 16% and 31.5% for trace elements. All values are presented as the mean of the duplicates.

The anthropogenic contribution of Pb was calculated with enrichment factors according to Boës et al. (2011). That is, Pb relative to a conservative element and a background value, in turn relative to the measured sample values. The calculation steps are outlined in equations 1 and 2. The background value was chosen as the mean of the most conservative part of the Pb and Zr (5.8 ppm and 120.5 ppm, respectively), hence using Zr as the conservative reference.

$$Pb_{EF} = \left(\frac{Pb_{sample}}{Ref_{sample}}\right)/\left(\frac{Pb_{backgd.}}{Ref_{backgd.}}\right) \quad (1)$$

$$Pb_{anth.EF} = \left(\frac{Pb_{sample} - \frac{Pb_{backgd.}}{Pb_{EF}}}{Pb_{sample}}\right) \cdot Pb_{sample} \quad (2)$$

2.3.4 Palaeomagnetic methods

The freeze core samples were analysed for mass specific magnetic susceptibility (χ) in a Geofyzica Brno KLY-2 susceptibility meter in the range 1-5 and χ (m^3 kg^{-1}) was calculated as 10^{-6}(0.01κ/g dry sediment) (Dearing 1994). The samples later received a direct current (DC) magnetization of 1T in a Redcliffe model BSM-700 pulse magnetizer (100 mT - 4 T) and the magnetic field strength was measured on a Molspin Minispin magnetometer. The minispin data was converted to SI units (Am^2) and the saturation isothermal remanent magnetization (SIRM) was calculated by correcting for volume and mass (from here on referred to as σSIRM). All measurements were performed on naturally wet samples. All samples were later freeze dried and water content was measured.

The piston core samples were first subjected to χ and σSIRM measurements as described above. After saturation, reversed and weaker fields (IRM_{-x}) were applied to the sediments and the ratios IRM_{-x}/SIRM were calculated for reversed field strengths of IRM_{-x} = 0.1 T and 0.3 T. Similarly, the "hard" isothermal remanent magnetization (HIRM) was calculated as 0.5($IRM_{-0.3T}$ + SIRM). Measured accuracy and precision for the method were within 0.1 and 0.09 %, respectively. Accuracy and precision for the χ measurements were within 0,03 and 0,09 %, respectively.

Natural remanent magnetization (NRM) was measured on a 2-G Enterprises long core superconducting rock magnetometer (model 755-R) in discrete sample mode and stepwise AF demagnetization at 5, 10, 15, 20, 30, 40, 50, 60 and 80 mT. Anhysteric remanent magnetization (ARM) was induced in a bias DC field superimposed on a 80 mT peak AF which was cycled to zero along the z-axis. All NRM and ARM measurements were conducted using a three axis direct current superconducting quantum interference device (dc SQUID) at the palaeomagnetic laboratory at the Department of Geology, Lund University. Palaeointensity was calculated as $NRM_{Jtot30mT}/ARM_{Jtot30mT}$.

Zijderveld orthogonal plots (Zijderveld 1967) and maximum angular deviation (MAD) values were calculated using Lund Palaeomagnetic Lab's EasyZijder 0.82, using PCA analysis following Kirschvink (1980) .

2.3.5 Dating techniques

The 7 cm^3 sample cubes were transferred to the composite depth scale by simply adding the interval to and from each core. Inclination and declination were plotted against depth in Matlab's app "Curve Fitting Tool" and the x-values (depth) at prominent features after a nonparametric smoothing spline had been applied were correlated to the corresponding ages in the reference datasets for inclination and declination (ARCH3k, pfm9k.1a and FENNOSTACK) (Snowball et al. 2007, Nilsson et al. 2014, Korte et al. 2009). The same technique was used to correlate between palaeointensity data and the FENNORPIS master curve (Snowball et al. 2007). The derived depth to age relationship of inclination, declination and pollution Pb marker horizons constituted the basis of an age model constructed in the Bacon v.2.2 R module (Blaauw & Christen 2011).

The ^{210}Pb analysis was conducted on a Ortec GEM series gamma spectrometer fitted with a high-purity germanium detector for around 3 days per sample at the Department of Geology, Lund University.

The sampled and identified terrestrial plant remains (0.6 mg *Betula spp.* catkin scales) were analysed for ^{14}C amount in an accelerator mass spectrometer at the Department of Geology, Lund University radiocarbon lab.

Table 1. Lithostratigraphic description of the Lake Storsjön sediment sequence.

Unit	Depth range (m)	Description	Notes
III	0-3.54	Clay gyttja banded with black layers. Dark brown color dominates but grades into a light grey tone towards the bottom.	Marked concretions of vivianite around organic remains at 1.71, 1.83, 2.31 & 3.27 m. 22 organic macrofossils found.
II	3.54-3.99	Laminated dark grey clays with thin laminations in the top and larger towards the bottom.	Laminations disturbed between 3.93-3.96 m
I	3.99-5.93	Dark grey diamictic sediments of varying composistion.	Casually interrupted stratigraphy of >5 cm inclusions of laminated clays

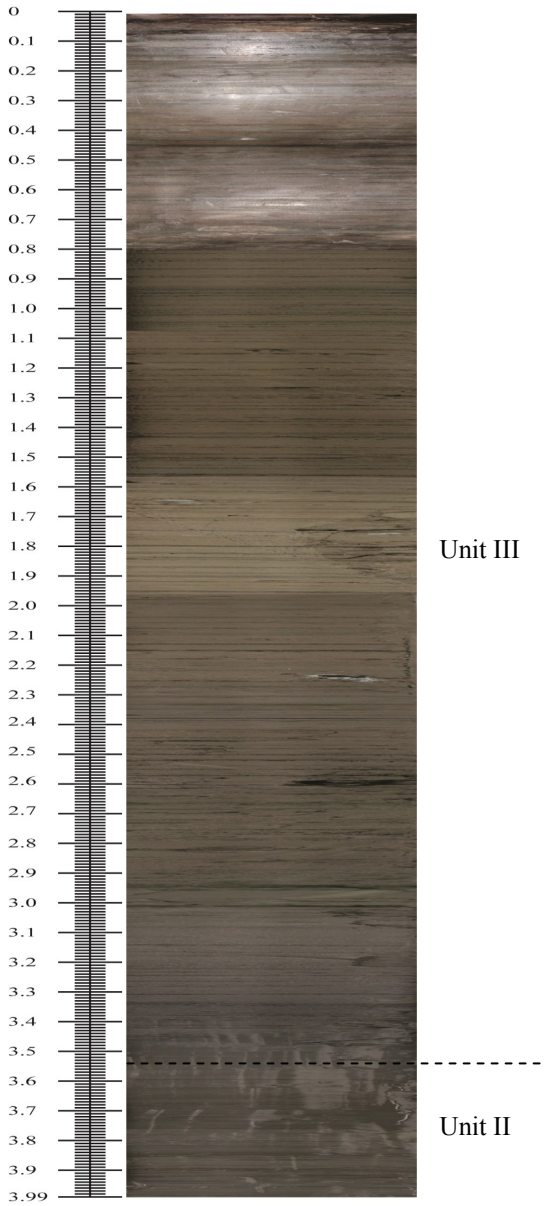

Figure 5. Composite lithostratigraphy of the subsampled units (units II & III).

3 Results

3.1 Sediment description and correlation

The composite depth sediment sequence equals 5.93 m of which 3.99 m was subsampled. The sediment sequence was divided into three lithostratigraphic units differentiating themselves significantly from each other (table 1). Composite sampled sequence photography is found in figure 5.

Unit I comprises the lower 5.93-3.99 m of the sequence and begins with 18 cm of dark grey, homogenous clay, only interrupted by two 1-cm bands of light grey clayey material. At 4.18 m depth a sharp transition to a dark grey sandy diamicton occurs which persist throughout the remainder of the unit. Variations within the unit do occur, however, where the diamict material is interrupted by typically >5 cm thick sections of laminated clays. Also grain size varies within the unit, ranging from sandy diamicton to gravelly, although the colour remains as a dark grey tone.

Unit II comprises a relatively short portion of the sequence and is found starting at 3.54 m depth and ending at the last sampled level of the sequence (3.99 m). This unit is a predominately grey clayey unit with intense banding. The bands are of a varying dark to bright grey character and span typically 1-2 mm in the upper parts of the unit and gradually grows larger further down in the unit. These bands, or laminations at the end of the unit are apparently disturbed at 3.93-3.96 m depth.

Unit III comprises the upper 3.54 m of the sequence, displaying a dark brown to light grey clay gyttja. The unit is banded by dark, almost black horizontal streaks occurring in varying frequency and width. The black bands appear to have a relatively coarser grain size and do not always spread out evenly over the exposed horizontal surface of the cut sediment. At around 3.3 m depth the black bands take on a more green tone while the overall sediment colour fades into a more grey tone. The now greenish bands are less pronounced and spaced further way from each other and also increase in width down to the end of the unit. At 3.27, 2.31, 1.83 and 1.71 m depth, distinct concretions of white vivianite are found around organic remains which later oxidized to become deep blue. Organic remains in turn, of terrestrial origin, were sparsely spread out (only in unit III) on the surface of the cut sediment sequence.

Water content (Fig. 6) deviates significantly between the freeze core and the piston cores. The upper part of the freeze core was close to 100 % water content (98,9 %) at 0.035 m depth while the uppermost piston core sample only contained 46,7 % water at 0.015 m depth. The trend continues downcore where water content of the freeze core never drops below 70

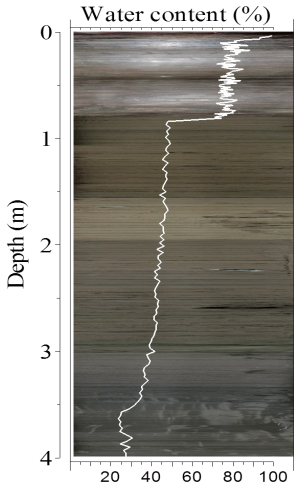

Figure 6. Water content (%) of the complete sampled sediment sequence. Note the large difference between the freeze core (upper 0.81 m) and the piston cores.

% (total depth of 0.85 m) and the piston cores remains around 45 % water content through the upper 2.01 m depth where after it declines downcore to stabilize around 25 %.

The piston cores were correlated to each other by means of lithostratigraphic alignment. The dark banding proved useful to ascertain a reliable core-correlation since the banding seems to have a uniform distribution over the sampled area. In the homogenous, diamicton parts of unit I, visual core-correlation was rendered obsolete due to the lack of lithostratigraphic variance. In these cases the cores were simply correlated by half core length overlaps.

The freeze core was difficult to correlate with the piston cores by visual alignment. Part of the problem is thought to stem from differential compaction exhibited by the two coring devices upon extrusion from the lake bed. Core correlation was thereby accomplished by correlations with LOI and elemental concentration of potassium (K) which proved to be closely covariant between overlapping cores (Fig. 7). However, core-correlation in this manner was only made possible by assuming a 0.105 m surface sediment loss from the piston core. This assumption is plausible since the technique suffers from relatively less delicacy of the procedure than do the freeze coring device. Hence, the freeze core was transferred into the composite depth scale at 0.81 m depth, corresponding to 0.915 m depth of the surface piston core.

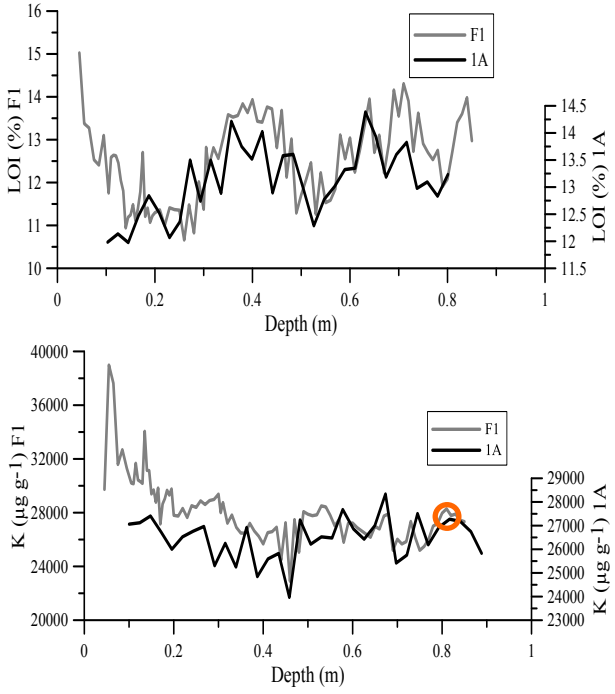

Figure 7. Correlation of LOI and Potassium between the freeze (F1) core and the uppermost piston core (1A). Orange marker denote the point of transfer from the freeze core to the composite depth scale.

3.2 Loss on ignition

Between 3.99-3.54 m the LOI is low and stable around 4 % where after inclining values takes on (4.7-12.9%) between 3.54-1.83 m (Fig. 8). Between 1.83 m and 0 m the LOI is fairly constant around 12.5 % except for minor variations in the upper 0.6 m of the sequence. The highest LOI in the sequence (15 %) is found at the uppermost sampled level (0.045 m).

3.3 X-ray fluorescence

The XRF data are plotted over the lithostratigraphy against depth together with selected elemental ratios and LOI in figure 8. No values of elemental ratios are presented in the text below.

The lithogenic elements titanium and zirconium (Ti and Zr) share a similar pattern of a decreasing trend from the bottom of the sampled sequence up to around mid-sequence where after they increase toward the top of the sequence. Below 3.54 m depth, the trend is stable for both elements and Zr stabilizes at near constant concentrations (150 ppm). Ti merely breaks the increasing trend and varies little down to the bottom of the sequence. Elemental ratios of Zr/Ti and Zr/K both show the same pattern, low values below 3.54 m and increase significantly between 3.54-3.33 m where after the ratios remain stable up to around 0.56 m, above of which they decrease towards the surface of the sequence. The Zr/Ti ratio decreases to some extent between 3.99-3.54 m while the Zr/K ratio is more variable over the interval, reaching its lowest value in the sequence at 3.81 m depth. Interestingly enough, the minor peaks at for example 2.58, 2.22 and 1.17 m in the Zr/K ratio coincide with the appearance of black bands within the stratigraphy (Fig. 21). This is also visible in the Zr/Ti ratio, but less pronounced.

Calcium (Ca) concentrations exhibit a highly variable concentration from the bottom of the sequence up to around 3.57 m, peaking within the interval at 11700 ppm. After 3.57 m, Ca concentrations remain stable around 5500 ppm up to around 0.43 m where an increasing trend towards the top begins, peaking near the surface at 8787 ppm. From the bottom up to 3.54 m sulfur (S) concentrations are rather stable but with a decreasing trend towards the top of the interval. Above 3.54 m a period of large concentration peaks emerges between 3.51-2.22 m, having largest peaks at 3.45 m (4662 ppm), 3.06 m (3504 ppm) and 2.79 m (3151 ppm). The stable period above 2.22 m up to the surface exhibits a mean concentration of about 1120 ppm only interrupted by a peak at 0.095 m (2500 ppm). Stable values of the 3.99-3.54 m interval is also found in the Mo/Al ratio after which two large peaks in the ratio is found at 3.45 m and 3.06 m with minor fluctuations in between. From 3.06 m and upward, the ratio experiences a rather stable and gentle incline, interrupted by a prominent increasing trend above 0.11 m. The Mn/Fe ratio is high and variable at the 3.99-3.54 m interval after which it experiences a rather stable increasing trend towards the surface of the sequence. Minor peaks are found but are generally

composed of a single data point. In the uppermost parts, the ratio increases its slope of the general increase.

The airborne trace metals copper (Cu), zink (Zn), arsenic (As) and lead (Pb) all show most elevated concentrations in the uppermost part of the sequence (upper 0.35 m). Pb have experienced a slight increasing trend from around 0.75 m depth, but exhibits its largest rate of change between 0.26 and 0.095 m. Downcore, concentrations of Zn, As and Pb are low and stable. Cu does however exhibit two concentration peaks lower down in the core, one at 3.24 m (74 ppm) and the second at 3.45 m depth (75 ppm). All the airborne trace metals exhibit a concentration incline in the upper parts of the freeze core. The concentrations start to increase almost simultaneously for Zn and As above 0.18 m while Cu concentrations start to increase above 0.24 m. Cu, Zn and Pb reach peak concentration at 0.095 m depth (100, 527 and 206 ppm, respectively) while As peaks higher up in the sequence (0.065 m, 200 ppm).

Calculated anthropogenic Pb reached highest concentrations at 0.095 m (187 ppm), corresponding well with the AD 1975 peak in Pb derived from the extensive use of leaded petrol at the time (Brännvall et al. 1999). Smaller but distinct peaks can be found at 0.22 m (15 ppm) and 0.4 m (10.6 ppm) (Fig. 9). The peaks were correlated with pollution Pb records from Västmanland (Lake Kalven) and Västerbotten (Lake Kassjön) (Fig. 1) corresponding to the increased metallurgy in mainland Europe and the UK (Bindler et al. 2009 & Brännvall et al. 1999).

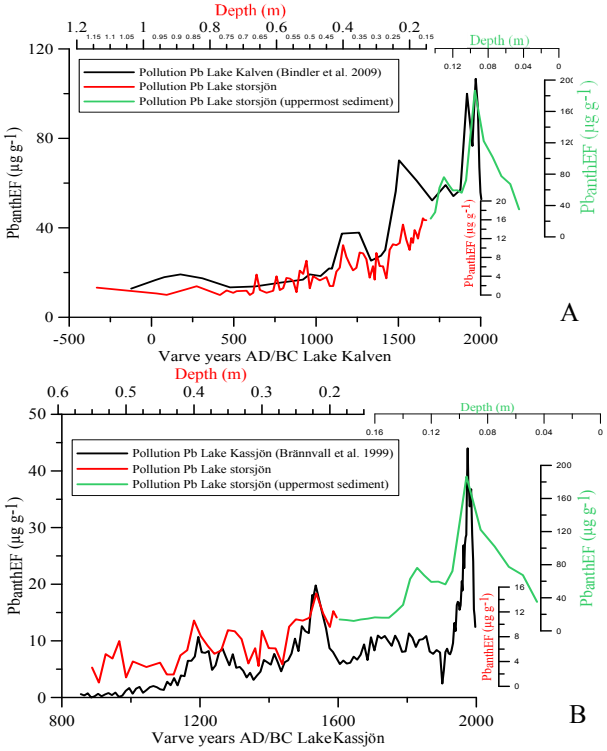

Figure 9.Pollution Pb age correlations with datasets from lake sediments 370 km south (A) and 300 km north (B) of Lake Storsjön, respectively.

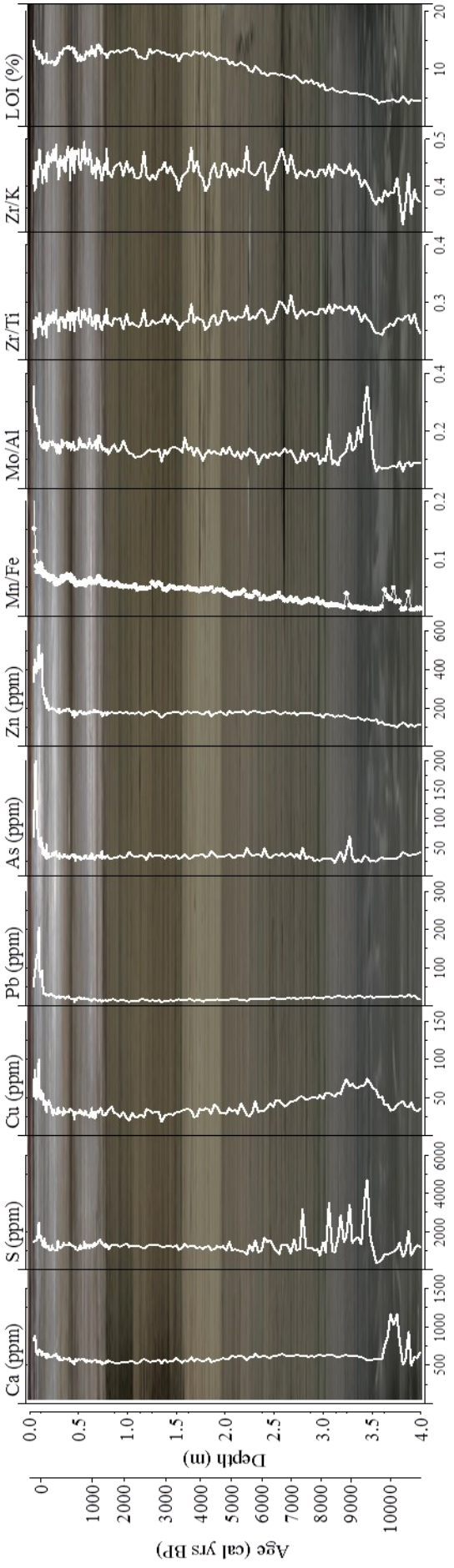

Figure 8. XRF concentration data and LOI superimposed on the lithostratigraphy.

3.4 Mineral magnetic parameters

Mineral magnetic parameters are presented graphically in figures 10 & 11.

The discrete sample susceptibility varied between 0.058 and 0.31 $10^{-6}m^3$ kg^{-1}, with distinct peaks at 3.45, (0.25 $10^{-6}m^3$ kg^{-1}), 3.06 (0.30 $10^{-6}m^3$ kg^{-1}), 0.74 m, 0.58 m, 0.48 m and 0.31 m (~0.31 $10^{-6}m^3$ kg^{-1}). The upper two data points at 0.035 and 0.045 m are erroneous and yielded negative values which cannot be trusted due to the high water content in these samples. After the peak in χ at 3.06 m the χ trend slightly decline towards the surface up to where the freeze core part of the sequence begin. Susceptibility is generally higher in the freeze core part of the sequence, but also more variable, the latter due to the difference in sample resolution. However, a slightly decreasing trend in the uppermost part of the freeze core (upper 0.3 m) can be discerned.

σSIRM values spanned between 0.23 and 7.08 mAm^2 kg^{-1} with two distinct peaks at 3.45 m (5.18 mAm^2 kg^{-1}), 3.06 m (7.08 mAm^2 kg^{-1}) and 0.29 m (5.23 mAm^2 kg^{-1}) depth. In the interval 3.99-3.54 m, the σSIRM trend is very invariable although rather high. Above this point a general increase begins, interrupted by the large peaks at 3.45 and 3.06 m. The increasing trend breaks only after 0.29 m where a decreasing trend takes on up to the surface of the sequence. During the general increase between 3.54-0.29 m small wiggles are visible but relatively small in comparison with the large peaks lower down in the sequence. The σSIRM/χ ratio varies between 5.62 and 30.82 kA m^{-1} with two distinct peaks at the same depths as the lower σSIRM record (Fig. 10) and one close to the surface of the sequence (0.055 m, 30.82 kA m^{-1}). Due to the negative χ values measured in the uppermost two samples, the upper two σSIRM/χ values are also negative and erroneous. The σSIRM/χ ratio basically displays the same pattern as the σSIRM curve, only bridging the gap between the freeze core and the piston cores. It also smoothens the amplitude of peaks seen in both χ and σSIRM. One peak however, increases in amplitude, namely the 0.055 m peak (30.82 kA m^{-1}).

The only clear stratigraphic marker in the sequence, namely the border to the laminated clays at 3.54 m is clearly visible in the mineral magnetic parameters as a transition from a stable trend to a changing one. The $IRM_{-0.3T}$ (S-ratio) displays four low peaks at 3.87, 3.48, 3.42 and 3.06 m but remains close to unity (1) for the remainder of the sequence (Fig. 11). The $IRM_{-0.1T}$ record display largely the same pattern, peaking at the same levels but the upper 3 m of the record exhibits lower values. The 'hard' isothermal remanent magnetization (HIRM, 0.5*($IRM_{-0.3T}$ + SIRM)) peaks at the same levels as the two S-ratios but in higher and reversed magnitude (448-1056 mAm^2 kg^{-1}).

3.5 Palaeomagnetic secular variations

The PSV data were correlated with three different datasets where the corresponding age of an event was transferred to the depth scale of the analysed sediments. For the most recent 3000 cal yrs BP, the

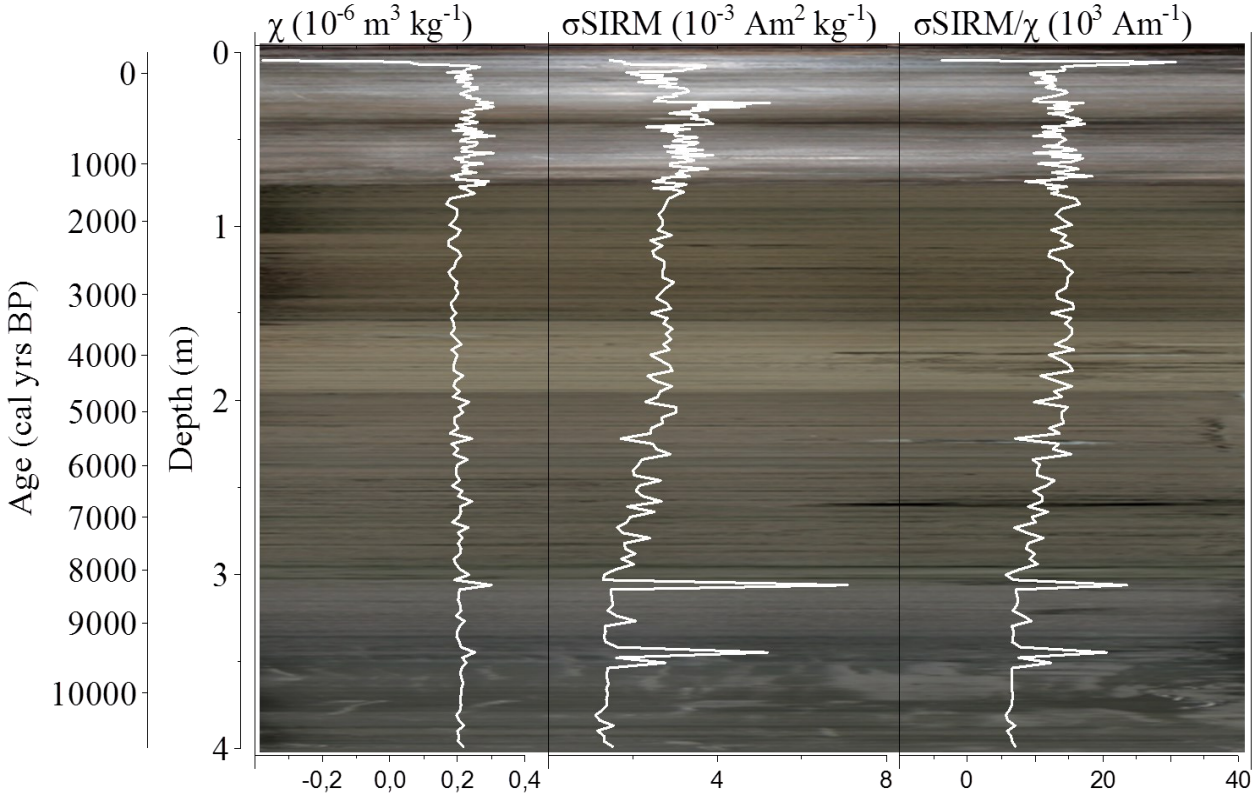

Figure 10. Mineral magnetic susceptibility, saturation isothermal remanence and the ratio of the both.

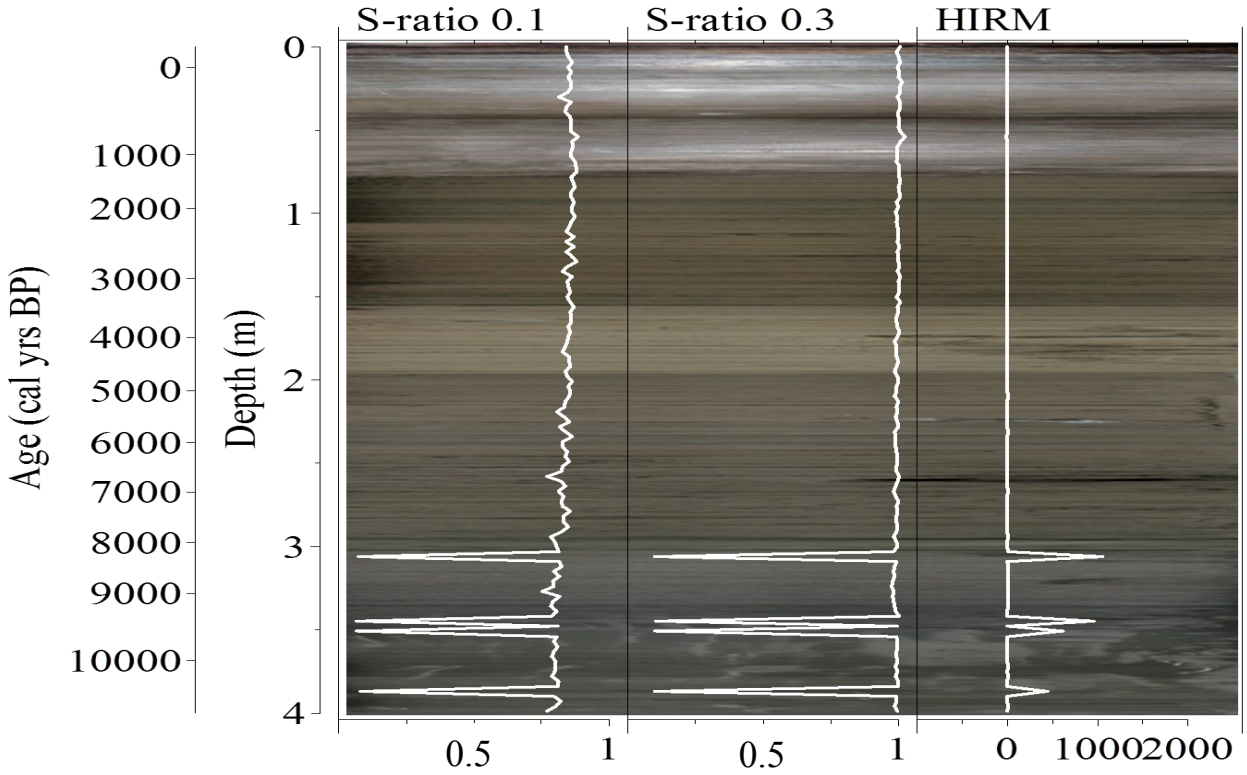

Figure 11. S-ratios for backfields of 0.1 & 0.3 T as well as HIRM.

ARCH3k archaeomagnetic curve (Korte et al. 2009) was used while the remaining part of the sequence was correlated with a combination of the pfm9k.1a curve (Nilsson et al. 2014) and the stacked datasets of FENNOSTACK (Snowball et al. 2007). Data from the ARCH3k and pfm9k.1a were modeled data of geomagnetic dipole (GDP) variations (Nilsson et al. 2014) with coordinate input of latitude=63.1º and longitude=14.4º and a spatial reach of both archaeomagnetic and palaeomagnetic (sediment) data within a 3000 km radius of the input coordinates. Palaeointensity was only correlated with the FENNORPIS data set (Snowball et al. 2007).

The NRM_{30mT} intensity signal (Fig. 12) varied between 2 and 43.9 mA m^{-1}. The signal was highly variable but a general pattern of lower intensity in the bottom parts of the sequence can be discerned. Largest intensity is found in two areas of the sequence. The first one between ~3-2.6 m and the second one between 1.8-0.8 m of the sequence.

The inclination varied between 20.2^0 and 83.5^0, the declination between 99.7^0 and 330.7^0 and the palaeointesnity between 0.12 and 2.7 (Fig. 12). Inclination shows a slightly increasing trend from bottom to top, where the most pronounced peaks are found in the upper 1.3 m of the sequence. Declination data exhibit a very steep gradient between 1.14 m and 1.32 m (119.6 -330.7^0) unprecedented by any other changes in PSV within the sequence. The palaeointensity is most variable in the upper part of the sequence, but exhibits large variations also in the bottom part of the sequence. Average values of inclination, declination and palaeointensity were 71.5^0, 191.5^0 and 1.5, respectively (Fig. 12).

The Zijderveld plots (Fig. 13) indicate a stable NRM signal, demagnetizing towards the origin (pers. Comm. Bryan Lougheed). This stability is also reflected in the maximum angular deviation (Fig. 12) (MAD) Typically, MAD values of five or lower were found, which is indicative of a very stable directional component.

The median destructive field (MDF) of NRM as derived from the AF demagnetization curves (Fig. 13) is lower in the pre-drainage sediments and increase rather steeply afterwards up to around 2.8 m. Above this level the MDF is stable (especially above 2.2 m) with only minor variations within (stable around 52 mT) throughout the sequence.

In the correlation with FENNOSTACK inclination data matches were found at 2.16 m, 2.52 m and 3.99 m corresponding to 5200, 6710 and 10060 cal yrs BP, respectively (Fig. 14). In the correlation with modeled data from the pfm9k.1a curve, matches were found at 1.65 m, 2,34 m, 3.09 m, and 3.63 m corresponding to 3200, 5630, 7770 and 9270 cal yrs BP (Fig. 15).

In the correlation with the modeled archaeomagnetic data of the ARCH3k curve, three age to depth tie-points were selected from the declination dataset. These were located at 0.55 m, 1.14 m and 1.32 m corresponding to 1290, 2250 and 2700 cal yrs BP, respectively (Fig. 16).

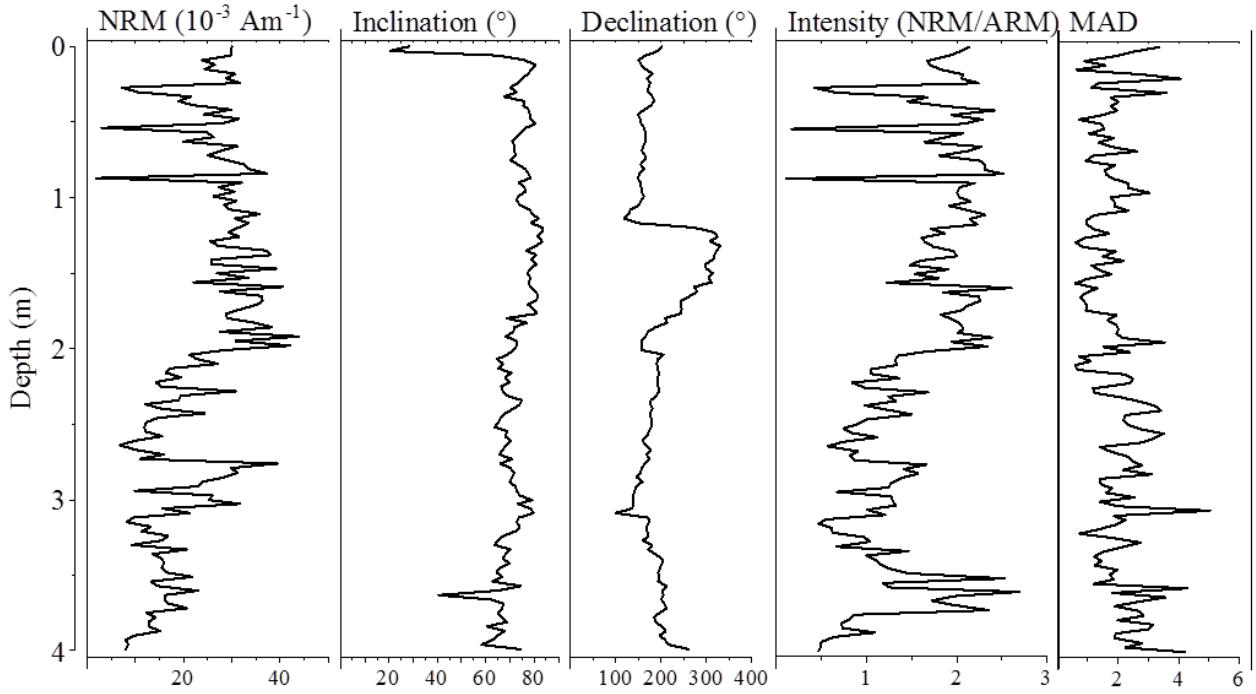

Figure 12. NRM intensity, inclination between 0-90°, declination between 0-360°, palaeointensity and maximum angular deviation (MAD) with depth. Note the very low MAD values during the steep change in declination at around 1 m depth.

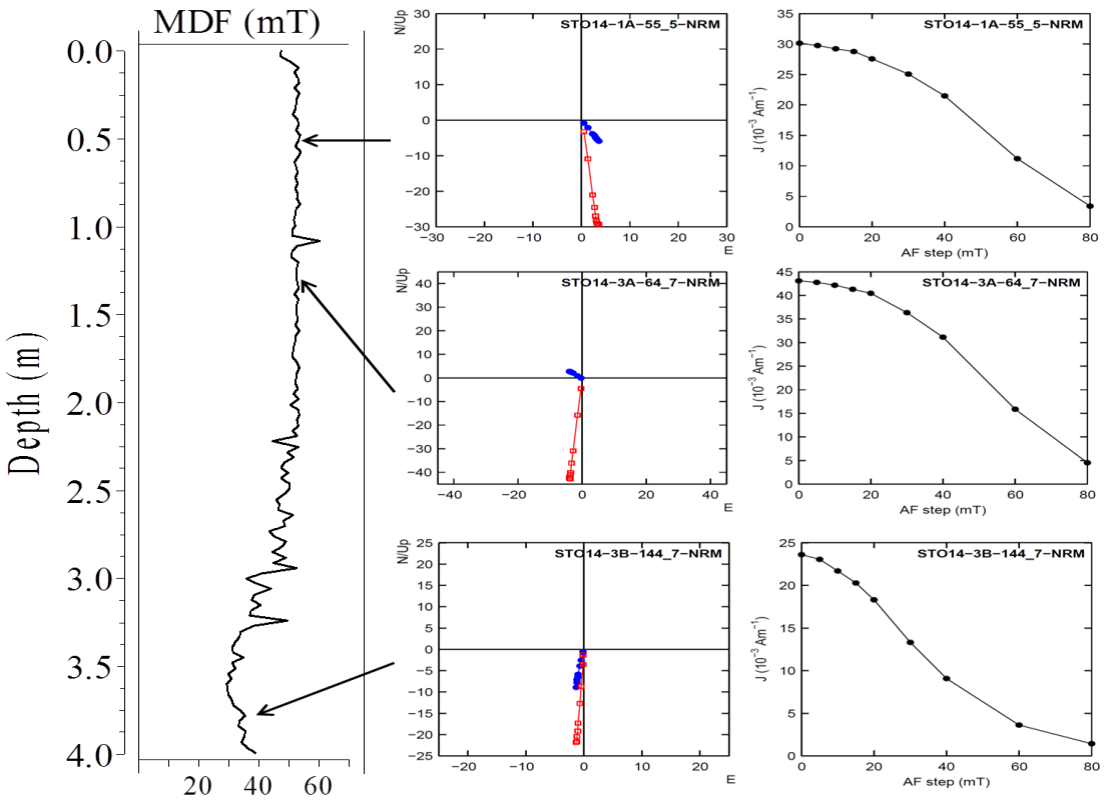

Figure 13. Median destructive field (MDF), Ziijderveld plots and associated AF demagnetization curves for three typical pilot samples with denoted position in the sediment sequence. The Zijderveld plots clearly demonstrate the consistent stable single-component NRM throughout the sediment sequence, both in pre-drainage samples as well as post-drainage samples. The MDF is lower in the pre-drainage sediments and near total stability of MDF is reached above 2.2 m depth (5400 cal yrs BP).

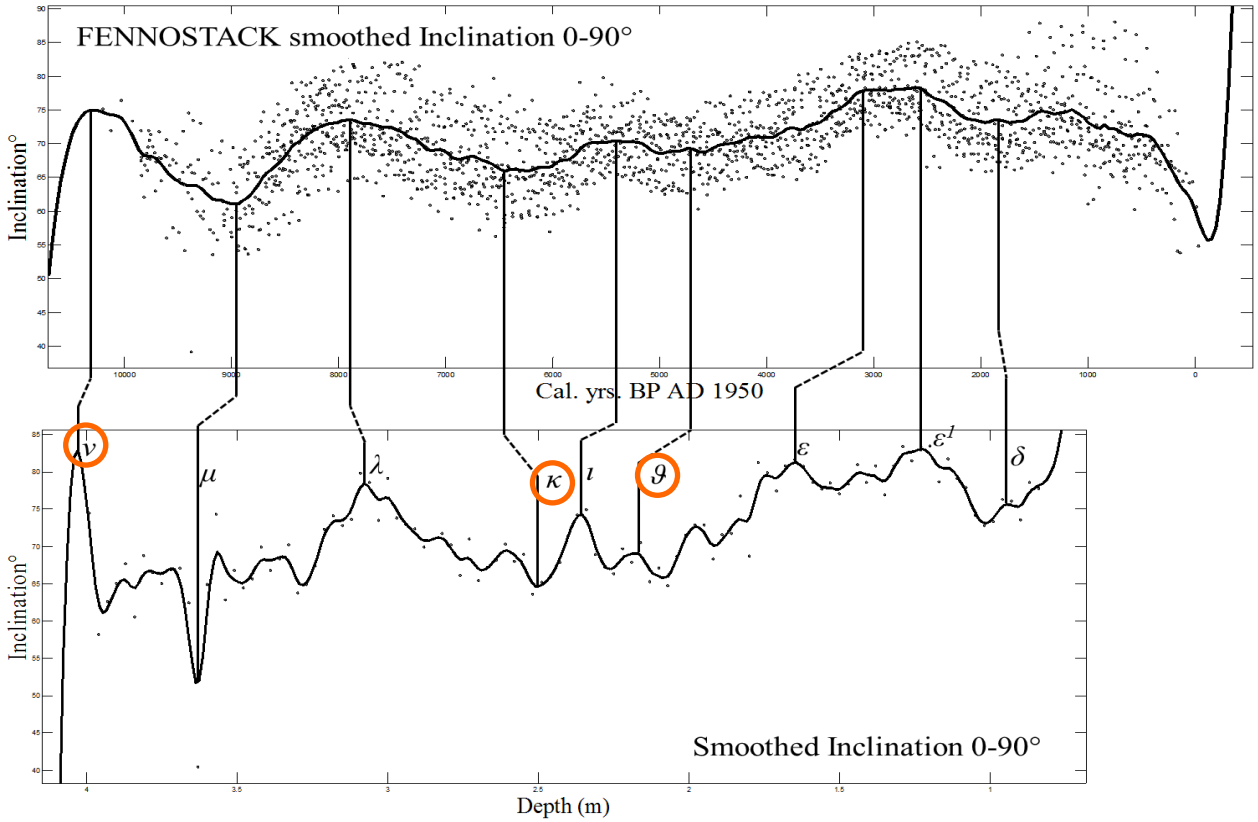

Figure 14. Inclination age-depth correlation with the FENNOSTACK stacked mastercurve of inclination. Greek letters denote prominent features as depicted by Snowball et al. (2007). Highlighted event are used in the age model.

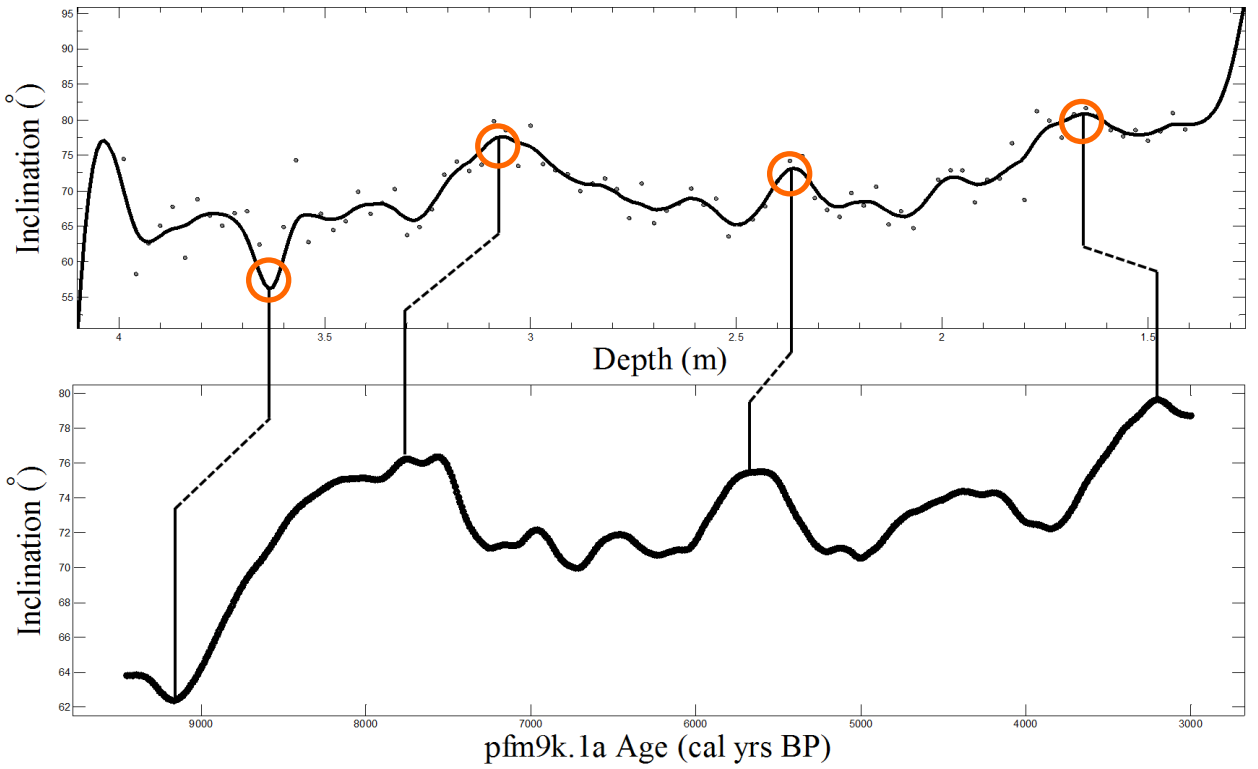

Figure 15. Inclination age-depth correlation with the pfm9k.1a inclination model for Lake Storsjön for the interval 3000– 9500 cal yrs BP. Highlighted features are used in the age model.

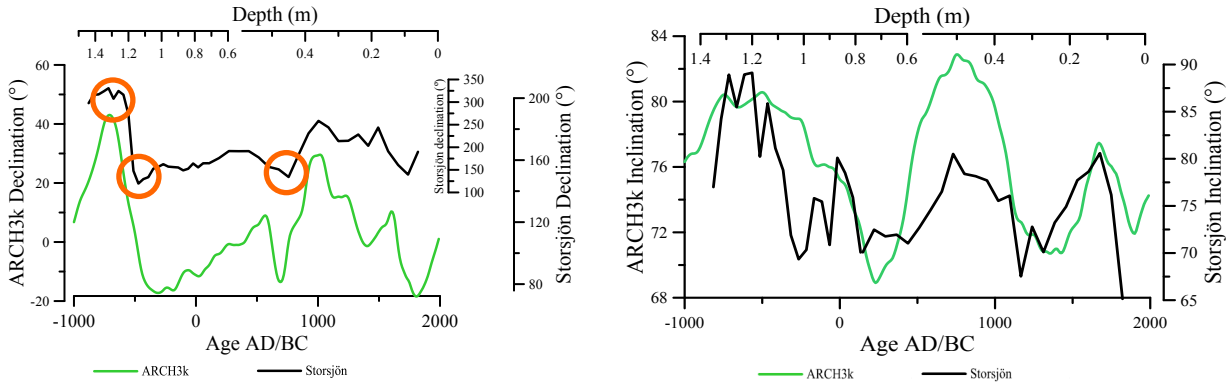

Figure 16. Declination and inclination depth to age correlations between the ARCH3k curve (green line) and the Lake Storsjön dataset (black line). Highlighted features are used in the age model. Note that only declination values were used for the upper 3000 cal yrs BP.

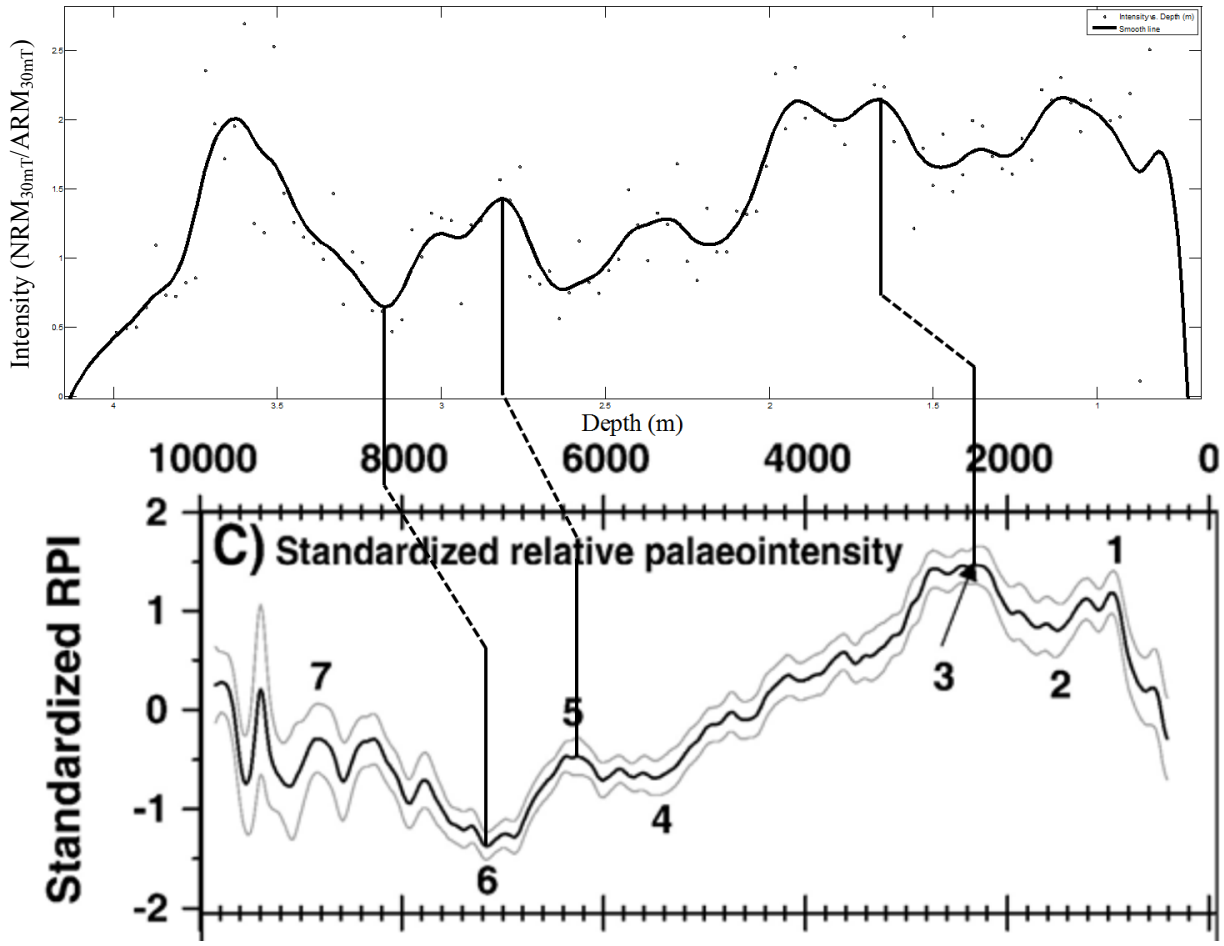

Figure 17. Possible chronomarkers for palaeointensity with the FENNORPIS stacked relative palaeointensity (RPI) record from Snowball et al. (2007). The FENNORPIS RPI have generally less validity to its denoted events (see Snowball et al 2007) and was hence never used in the construction of the age model. However, three events (3, 5 & 6) can be determined to match with reasonable certainty to the palaeointensity of the Lake Storsjön records.

Palaeointensity correlation with the FENNORPIS stacked dataset (Fig. 17) holds less validity to its denoted events (see Snowball et al. 2007) and was thus not used in the age model. However, similarities between the two curves can be discerned at the 3 (2175 cal yrs BP), 5 (6120 cal yrs BP) and 6 (6600 cal yrs BP) events corresponding to 1.4, 2.8 and 3.2 m, respectively. The tiepoints was however not evaluated further.

3.6 ^{210}Pb dating

The ^{210}Pb analysis suffered from insufficient sample sizes and thus produced unreliable age estimates. Total ^{210}Pb activity ranged from 83 to 623 Bq kg^{-1} and

the excess ^{210}Pb between 25 and 619 Bq kg^{-1}. On the other hand, ^{137}Cs measurements, ranging from 0 to 2087 Bq kg^{-1}, produced a distinct peak at 0.05 m depth in the sediment sequence, most likely corresponding to the radiocaesium atmospheric enrichment in AD 1986 due to the Chernobyl power plant meltdown (Fig. 18). No other distinct features were found in the ^{210}Pb and ^{137}Cs record.

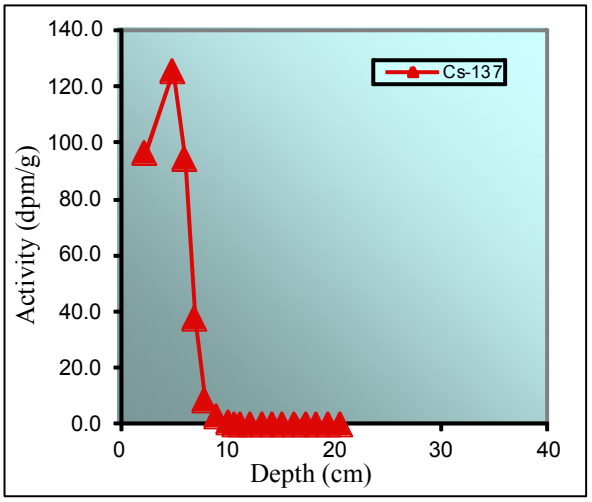

Figure 18. ^{137}Cs activity for the upper 20 cm of the freeze core. Note the prominent peak in activity at 0.05 cm depth.

3.7 ^{14}C dating

The radiocarbon date was derived from a wet sieved sample at 3.226 m depth. The organic remains were identified under a light microscope as *Betula* sp. Catkin scales in rather low quantities, equaling 0.6 mg carbon after acid wash (HCl). The resulting radiocarbon age of the sample was determined to be 8055 ± 45 radiocarbon years BP. The results are summarized in table 2.

3.8 Age model

The pollution Pb data provided three dates (AD 1975, 1530 and 1200) for the upper 0.4 meters of the freeze core. The pollution Pb peaks were correlated with an age using pollution Pb data from Bindler et al. (2009) and Brännvall et al. (1999).

PSV data provided 10 dates which are deemed reliable, derived from the combined correlation with ARCH3k, pfm9k.1a and FENNOSTACK stacked master curve, three dates from declination data (Fig. 16) and seven dates from inclination data (Fig. 14 & 15). Declination data were exclusively used for the younger part of the age model (e.g ARCH3k) while inclination data were used to construct the older parts. No dates derived from the palaeointensity were used due to high uncertainties in correlation. By combining the pollution Pb dates with the PSV dates, an age model was constructed independent of absolute dating with Bayesian interpolation between tiepoints (Fig. 19).

The ^{210}Pb dating produced unreliable dates and is therefore not presented in this paper. The ^{137}Cs activity in the samples was also low but exhibited one large peak in activity at 0.005 m depth (Fig. 18) which could be assigned an age (AD 1986).

The radiocarbon date was collected at 3.226 m depth and had an uncalibrated age of 8055 ± 45 ^{14}C yrs.

The final age model used as a chronology in this paper was constructed based on a combined model of relative (pollution Pb & PSV) and absolute dating techniques (radiocaesium & radicoarbon) and spans over 10,818 cal yrs BP. sedimentation rates were calculated as mm accumulated sediment per year and plotted below the corresponding age model (Fig. 19). Maximum sedimentation rates were found in the upper 0.1 m of the sequence, with rates up to 1.43 mm/yr. relatively high sedimentation rates were also found in the lowermost 0.7 m of the sequence at around 0.4 mm/yr. Minimum sedimentation rates were found between 3.2 and 1.6 m depth at around 0.3 mm/yr. Mean sedimentation rate was 0.39 mm/yr.

4 Discussion

4.1 Chronology

The three pollution Pb dates used in the age model provided some constraints of the upper part of the sediment sequence. However, a ^{210}Pb and ^{137}Cs approach generally produces a more precise age estimation of the upper part of a sequence due to the more narrow uncertainty envelopes and higher resolution. However the accuracy of ^{210}Pb and ^{137}Cs dating has been shown to be affected by, for example, within sediment diffusion. For example, Klaminder et al. (2012) showed that ^{137}Cs from the Chernobyl fallout marker horizon in a varved lake sediment sequence in northern Sweden migrated downcore and masked the nuclear bomb peak of AD 1964. Brenner et al. (2004) showed that ^{226}Radon (^{226}Ra) input due to urban sources or land use change in the catchment can complicate dating with ^{210}Pb by adsorption to the surface sediments, hence making reliable estimates of the supported fraction of ^{210}Pb complicated. Benoit & Rozan (2001) found different total inventories of ^{210}Pb in cores collected at the same place but 20 years apart, which would point to some remobilization of ^{210}Pb. The ^{210}Pb and ^{137}Cs dating technique therefore benefits from an independent age estimate, such as pollution Pb chronomarkers, and vice versa.

Table 2. Results summary of the radiocarbon dating

Lab id	^{14}C age	Sample mass (mg)	Pretreatment
LuS 11056	8055 ± 45	0.6	HCl

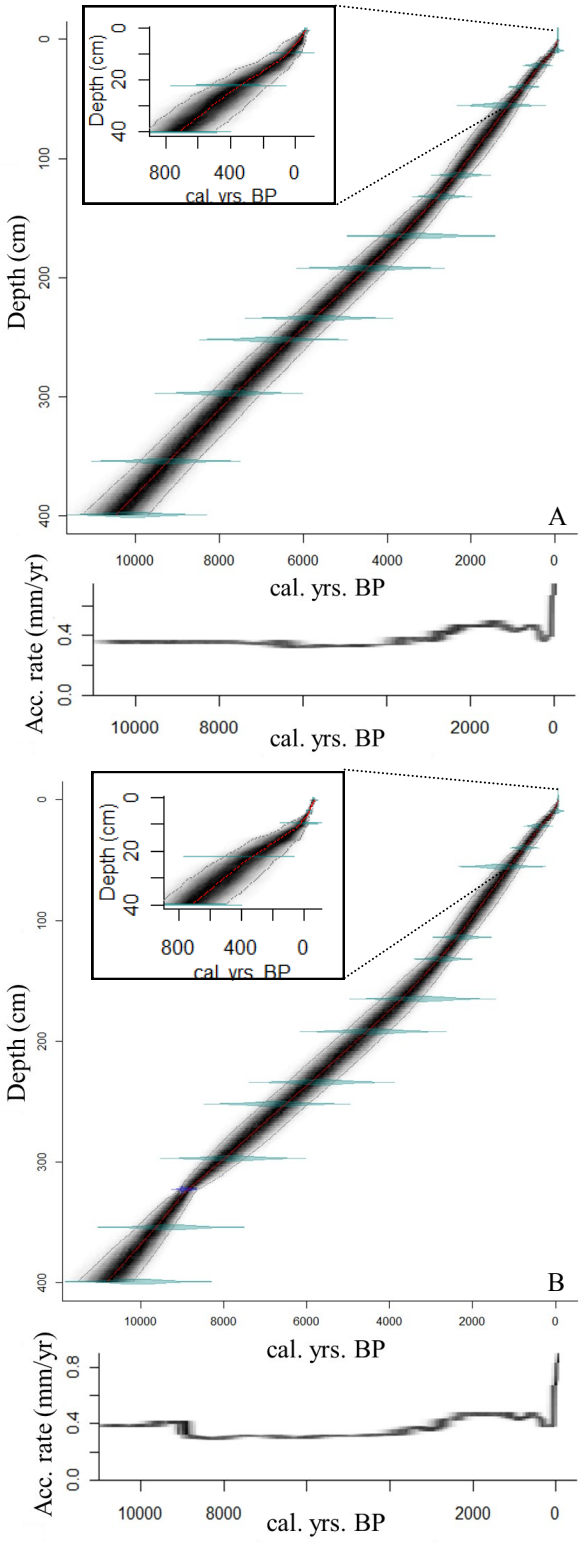

Figure 19. Age-Depth model with associated sedimentation rates for A) Pb-PSV model and B) Pb-PSV-^{14}C model. Boxed in is a zoomed up version of the age model for the pollution Pb dates (A) and the pollution Pb dates plus the radiocaesium date (B). Note the large difference in uncertainty when the radiocaesium date is included.

The pollution Pb age model was tested by inserting a PSV (declination) derived date from the ARCH3k curve (Nilsson et al. 2014) between the two lower pollution Pb markers. This however did not prove or disprove the pollution Pb date's validity but rather disproved the validity of the PSV date, which has a larger uncertainty envelope. The ARCH3k declination correlation yielded an age of 310 cal yrs BP at 0.12 m depth. When run in the age model together with the pollution Pb dates, the PSV date produced suspiciously low sedimentation rates, a behaviour which is not expected at the top of a sediment sequence. When the PSV date was excluded sedimentation rates rose and the existing pollution Pb dates again fell within the uncertainty range of the age model. The ^{137}Cs dating yielded one major peak in ^{137}Cs activity at 0.05 m depth, which with high confidence would reflect the Chernobyl accident in AD 1986. This date constitutes an important bridge between the Pb pollution date at AD 1975 and the surface (AD 2013). The ^{137}Cs date fits well in the chronology (Fig. 19) and increased the near surface sedimentation rate as would be expected. This date further validated the accuracy of the pollution Pb dating and contributed significantly to the overall age model.

The PSV part of the age model was constructed independent of ^{14}C measurements, based solely on correlation with ARCH3k and pfm9k.1a modeled data (Nilsson et al. 2014, Korte et al. 2009) as well as FENNOSTACK (Snowball et al. 2009) inclination and declination data. The input uncalibrated ages were evaluated by giving more weight to events with larger change in between tie point, hence assigning them more narrow uncertainty envelopes (e.g. declination events 2 & 3 in figure 16, ±200 yrs). Correlation tie points with less change in between tie points were assigned an error of 500 yrs (i.e all other PSV dates). The approach was further corroborated by investigating the MAD values. For example is the lowest MAD values to be found are just where the steepest change in declination occurs (Fig. 12).

The resulting Pb-PSV age model was tested by inserting the radiocarbon date at 3.226 m and running the age model again thus producing a second age model. The ages of the Pb-PSV-^{14}C model and the Pb-PSV model were plotted against each other in the depth range of 3-3.99 m, producing a coefficient of determination R^2=0.9977. The radiocarbon date is deemed reliable given the source material's terrestrial origin and excellent preservation. Hence the uncertainty envelopes are relatively smaller (±45 yrs) than the PSV dating errors and is considered as more reliable. At the evaluation of the age models, special attention is paid to the correspondence of sedimentation rates with changes in lithostratigraphy. The Pb-PSV age model produces a uniform sedimentation rate from the bottom of the sequence to around 6000 cal yrs BP where a small decrease occurs. The Pb-PSV-^{14}C age model on the other hand, displays a more variable sedimentation rate in the lower part of the sequence. Since the only

pronounced change in lithology occurs at 3.54 m, where the glaciolacustrine clay grades into a more organic deposit, a change in sedimentation rate around this level is expected (Allen 1999). The Pb-PSV-^{14}C model implies a subtle increase in sedimentation rate right around the border between unit II and III, most likely due to the newly exposed land in the surrounding catchment area, and later decreases distinctively between 9000-8700 cal yrs BP. A decline in sedimentation rate is expected to occur soon after the lake formation, as organic matter content increases and hence the compressibility of the deposit. However, this change is expected to be gradual, not sharp as implied by the sedimentation rate change. Reasons for the observed sharp change is most likely the differences in accuracy of the radiocarbon date as compared to the above and below PSV dates and possibly also an artifact of too low memory in the prior settings of the age model within the Bacon R module. The narrow uncertainty envelopes of the ^{14}C date relative to the adjacent PSV dates thus affected the slope of the curve, inducing the large discrepancy in sedimentation rates between the two age models. However, despite inconsistencies in the timing and rate of change of the sedimentation rate relative to the lithostratigraphy of the sediment sequence, better agreement is found between expected and modeled sedimentation rates when including the ^{14}C date in the Pb-PSV age model. The final age model for the Storsjön sediment sequence was thus chosen to be the Pb-PSV-^{14}C age model.

Both age models do experience a preference toward the older parts of the uncertainty envelope of the lowermost date (10,800). This could be due to the lack of sedimentation rate memory below the date hence making uncertainty fitting arbitrary. This is problematic since it contradicts the assumed dates of deglaciation proposed by Johnsen et al. (2010) who radiometrically dated glacial erratics on mountain tops to the west of the investigated area to have deglaciated around 10 600 ±600 cal yrs BP. Since the deglacial succession have been shown to move from west to east in this area (Lundqvist 1973), hence putting the mountainous areas to the west of Lake Storsjön in an earlier deglaciation stage, the lowermost date must be considered unreliable.

Additionally, the radiocarbon date was calibrated individually in OxCal v.4.2.4 (Bronks Ramsey 2009) against the same calibration curve as within the Bacon R module (IntCal 09) (Fig. 20). The radiocarbon date was found to be located on a plateau within the calibration curve and having a 2σ (95.2%) age probability distribution of 8768-9092 cal yrs BP. The calibrated age of the same date within the Pb-PSV-^{14}C age model was determined to be 8857 cal yrs BP which is well within the 2σ probability distribution, although with a preference towards the younger part of the plateau.

4.2 Coring techniques

The large discrepancy in water content between the freeze core and the piston cores highlights the difference of the two coring techniques (Fig. 6). Also, the loss of 0.105 m of surface sediments when using the piston core approach further elucidates the need for a combined coring approach. The freeze core provided three pollution Pb dates and one radiocaesium date while excluding one possible chronomarker from the PSV data that overlapped with the freeze core, namely the γ-event from the FENNOSTACK inclination data (see Snowball et al. 2007). However, as the three pollution Pb dates were less pronounced in the piston cores XRF data, the freeze core proved to be exceptionally useful in constructing an age model for the younger sediments.

The relatively tedious method of subsampling the freeze core, although precise and with the possibility for high resolution, was more time-consuming and costly than traditional gravity core subsampling. The differing degree of compaction in the freeze core relative to the piston cores also made lithostratigraphic correlation an issue, further highlighting the need for non-subjective correlation between cores.

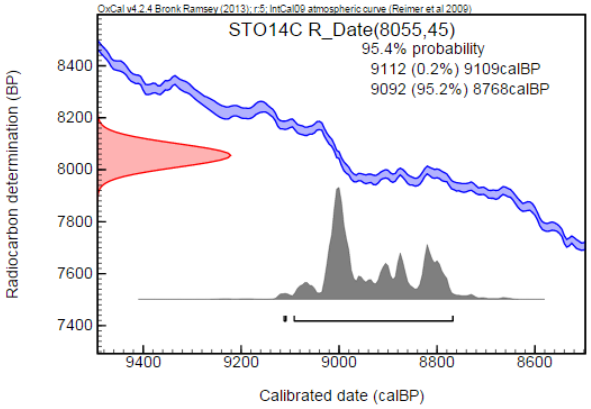

Figure 20. Single date calibration in OxCal v.4.2.4 of the radiocarbon date used in the final age model. Note the rather broad age probability distribution induced by the plateau in the calibration curve.

4.3 Early postglacial development

The invariable ocular appearance of the sediment sequence proves the lack of abrupt changes in the catchment area and within the lake itself. The only profound lithological change occurs at 3.54 m where the laminated clay of unit II transition into the homogeneous clay gyttja of unit III. The sediments below 3.54 m are interpreted as being laid down in an ice-distal environment of an ice dammed lake. The disappearance of the cyclic lamina above this point, with subsequent transition to a more present-day like sedimentation pattern indicates the drainage of such an ice dammed lake and the subsequent lake formation. According to the Pb-PSV-^{14}C age model this transition occurs 9629 cal yrs BP (Fig. 19B). As concluded by Borgström (1989), Lake Storsjön was covered by a complex of shifting ice lakes after the retreat of the Scandinavian ice sheet, which receded from the area at

around 10000 cal yrs BP. This means that the dead ice bodies left behind after the glacial recession persisted for about 400 years before the lake and the surrounding catchment was free of glacial influence.

The glaciolacustrine-lacustrine transition is also characterized by a change in proxy inferred grain size. The Zr/Ti ratio is decreasing slowly upward within the varved clay section (Fig. 8), indicating a fining upward. However, the Zr/K ratio display higher fluctuations within the section indicating that, in excess of for the increasing silt fraction upward, there are episodes of increasing clay content (Cuven et al. 2010, Taboada et al. 2005). It can also be concluded, based on the Ca concentrations, that the finer, mostly clastic material was derived from the surrounding catchment where the newly exposed ground of calcareous bedrock and soils reside (Fig. 2).

The transition from glaciolacustrine sedimentation is accompanied by a distinct rise in the Mo/Al ratio which in turn is accompanied by an equal rise in S concentrations. The Mo/Al ratio is commonly used as a proxy for palaeo-oxygenation of the sediments. The enrichment of Mo in sediments is frequently attributed lowered oxygen levels which in turn can be caused by several different processes (Dean et al. 1999). In this case the Mn/Fe ratio, indicative of palaeo-redox environments (Naeher et al. 2013) is high in the laminated section below 3.54 m, and drastically drops just above. One of the criteria for the preservation of varves is anoxic conditions, preventing burrowing biota to mix the sediments (Zolitschka 2007). However, the low LOI, cold waters and minerogenic domination most likely prevented the establishment of such biota, hence preserving the varved structure regardless of the oxic conditions. The decrease in sediment oxygenation above 3.54 m is related to the increase in LOI above this point. The Increase in LOI is modest (1.3 % between 3.54 m and 3.45 m), but might be masked by the increased sedimentation rate (Fig. 19). The increase in LOI, likely caused by the reduction of the glacial influence on the lake permitting primary production to flourish, caused the oxygen levels to drop due to oxygen consumption by bacterial respiration. This in turn forced the primary biota reducing sulfate as an energy source, a process with high affinity for Mo enrichment (Piper & Isaacs 1995).

The subsequent decrease in the Mo/Al ratio therefore represents the return of oxygenated conditions as further supported by the increasing Mn/Fe ratio. The increasing bottom water oxygenation could be due to increasing circulation in the basin as outlets became operative after the dead ice recession, namely the drainage of the Landö-issjön as proposed by Lundqvist (1973).

The 3.45 m (9400cal yrs BP) peak in Mo/Al ratio and S (Fig. 8) is accompanied by drastically increased values in σSIRM, σSIRM/χ and to a certain degree, χ (Fig. 10). The peak also coincides with a large positive peak in HIRM and an equally large reversed peak in the S-ratios (Fig. 11), suggesting that the decreased size of the mineral magnetic grains (as suggested by an increase in σSIRM/χ) also are "hard" single domain grains (Moskowitz 1991). Coupled with the inferred anoxic conditions, increasing LOI and large sulfur supply around this time (9400 cal yrs BP), the source of the mineral magnetic composition is here suggested to be bacterial greigite (Fe_3S_4) magnetosomes (Bazylinski 1996, Evans & Heller 2003). Lyons et al. (2001) found a similar pattern of increasing primary production, decreasing O_2 levels and higher Mo/Al ratio and S concentrations during the glacial-interglacial transition in the Cariaco basin. The study suggests, similar to this study, that the transitional conditions gave rise to extensive iron sulfide formation. However, Lyons et al (2001) attributed the iron sulfide increase to pyrite formation. In the case of Lake Storsjön, pyrite formation is less likely than greigite formation since pyrite is paramagnetic and would not yield the observed increase in the mineral magnetic properties (Moskowitz 1991, Thompson & Oldfield 1986).

The presence of magnetotactic bacterial greigite has previously been interpreted to represent episodes of anoxia in the Baltic Sea (Reinholdsson et al. 2013), which further elucidates the geochemical proxy indications found in the glaciolacustrine-lacustrine transition of Lake Storsjön. Furthermore, Snowball et al. (2002) found a positive linear relationship between the SIRM of northern Swedish lake sediments and organic content. This relationship is also evident in the sediments of Lake Storsjön, although not within the glacial clay unit (Fig. 21) where a negative relationship is found. The positive linear trend of σSIRM/LOI of the postglacial sediments is interrupted by three prominent outliers, displaying a much steeper positive trend. These outliers correspond to the above mentioned anomalies of increased anoxia and greigite formation. Although the organic content at these levels are low, they do represent significant increases from previous values. It is therefore hypothesized here, that the existing relationship between SIRM and organic matter is indeed coupled to changing redox conditions and favours magnetotactic bacterial greigite formation, but only where organic matter production increases significantly over a short period of time.

4.4 Lake development

Following the mineral magnetic assemblage upward, a large peak is found 8180 cal yrs BP, a feature also visible in the S-ratios and HIRM (Fig. 10 & 11). Furthermore, the Mo/Al ratio does as well peak at the same level as well as S concentrations just before (Fig. 8). This observed behaviour is similar to that of the transitional changes around 9400 cal yrs BP coupled to the isolation of the modern lake basin. However, no lithostratigraphic change can be found around this time. Instead, it is here proposed that circulation in the lake temporarily deteriorated as a response to prolonged ice cover during the 8.2 kyr cooling event. This in turn would explain the invariable LOI, low inferred

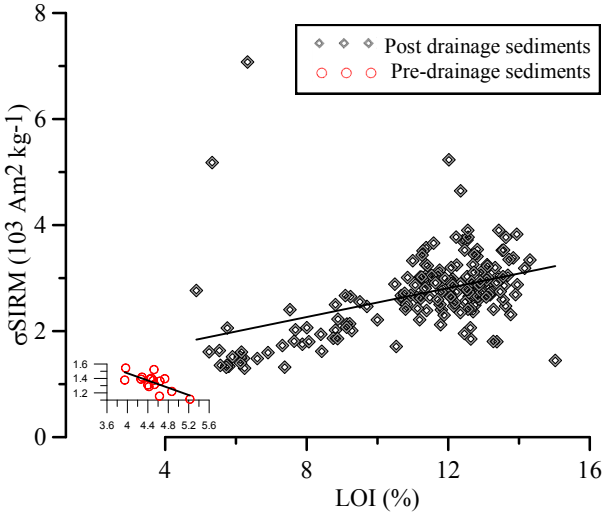

Figure 21. Linear relationships of σSIRM vs LOI. Note the differing trends of the two units.

oxygenation (Mo/Al ratio) and the increasingly sulfidic environment. The conditions that arose during this rather short-lived period then again promoted bacterial greigite formation similar to that of the glaciolacustrine-lacustrine transition, thus explaining the behaviour of the mineral magnetic record at this time. Evidence of the well-established cooling event around 8200 cal yrs BP have been brought forward by e.g. Alley et al. (1997), Nesje et al. (2001), Hammarlund et al. (2003) and Magny et al. (2003) and more locally by Bergman et al. (2004) and Hammarlund et al. (2004).

The remainder of the intermediate part of the sequence (c. 8000-4200 cal yrs BP) is characterised by little or no variation in both the geochemical and palaeomagnetic records (Fig. 8 & 10). LOI and the Mn/Fe ratio experience a steady and rather large incline during the interval together with a gentler incline in σSIRM and σSIRM/χ ratio while χ is declining slightly. The sedimentation rate remains remarkably stable and low throughout the whole period. The concentration dependent mineral magnetic parameter χ's decrease has to be interpreted as a dilution of the clastic detrital fraction as organic content increases. The σSIRM and σSIRM/χ ratio's increasing trend on the other hand indicate that the mineral magnetic assemblage becomes increasingly dominated by more fine grained stable single domain magnetite (Thompson & Oldfield 1986). Based on the positive linear relationship of σSIRM vs LOI (Fig. 21) and the results of Snowball et al. (2002) discussed above, the mineral magnetic assemblage during the period is believed to be of magnetotactic bacterial origin. However, the fossil magnetosomes are here interpreted as being composed of magnetite in contrast to greigite as suggested for the suboxic to anoxic events of the glaciolacustrine-lacustrine transition and the cooling event around 8200 cal yrs BP. Thus it is theorized that bacterial greigite forms preferentially during highly oxygen depleted environments while bacterial magnetite is favoured by increasing organic content in the presence of oxygen. The onset of the increasing trend in inferred magnetotactic magnetite coincide with a decreasing trend in the MAD values of the NRM (Fig. 12) which would imply that the carriers of the NRM used for directional PSV data in this study relies heavily on fossil magnetosomes which are carriers of a stable NRM signal (Snowball 1994). Furthermore, the MDF of NRM also stabilizes at higher values from around 8000 cal yrs BP and remains stable throughout the sequence. Since higher MDF of NRM indicate more stable carriers of NRM (Dankers 1981), this further elucidates the interpretation of magnetotactic magnetite being the major NRM carrier from 8000 cal yrs BP and onward. The observed development comes to halt above c. 4200 cal yrs BP corresponding well with the end of the Holocene thermal maximum (HTM) and a change toward more unstable climatic conditions (Jessen et al. 2005). This warmth period have been described by many authors, highlighting a disagreement in both timing and magnitude of the event(s). For example Renssen et al. (2009) puts the warmth period in Europe between 8000-5000 cal yrs BP while Seppä & Birks (2001) argue that the HTM culminated between 8200-6700 cal yrs BP. Furthermore, Eronen et al. (1999) suggest the period (8000-4000 cal yrs BP) to be a dry period while Bjune et al. (2004) argue that the same period was a humid one. Despite the many inconsistencies, the general trend of a warmth period during the interval remains solid. Judging from the sediment sequence of Lake Storsjön the period may be regarded as a period of warmer climate as inferred from the increasing LOI and of relative stability as suggested by the very stable sedimentation rate as well as the lack of variation in the mineral magnetic and geochemical records.

Another characteristic treat of the post-drainage sediments is the occurrence of black bands irregularly spaced and dimensioned throughout the sequence. The black bands, where subsampled, do not correspond to any change in LOI, mineral magnetic parameters or elemental concentrations. Moreover, no prominent black banding can be found at the levels of inferred suboxic to anoxic conditions with bacterial greigite formation. They do however correspond well with increases of the Zr/K elemental ratio peaks (Fig. 22), indicating a coarsening of the clastic fractions within the bands (Taboada et al. 2005). Upon closer inspection in 40x magnification in a light microscope the black bands seem to be relatively poorer in organic micro and macro fossils (Fig. 23). The bands later oxidized to become dark brown and relatively lighter in colour than the main constituent of the sediments. Odegaard et al. (2003) found that black layers established in sediments from the Great Lakes, United States had formed as a response to decreased circulation coupled to a lake level rise and warm and dry climate. The decreased circulation gave rise to suboxic to anoxic conditions where intense iron sulfide production took place. As described above, such climatic history is interpreted as being present during the time

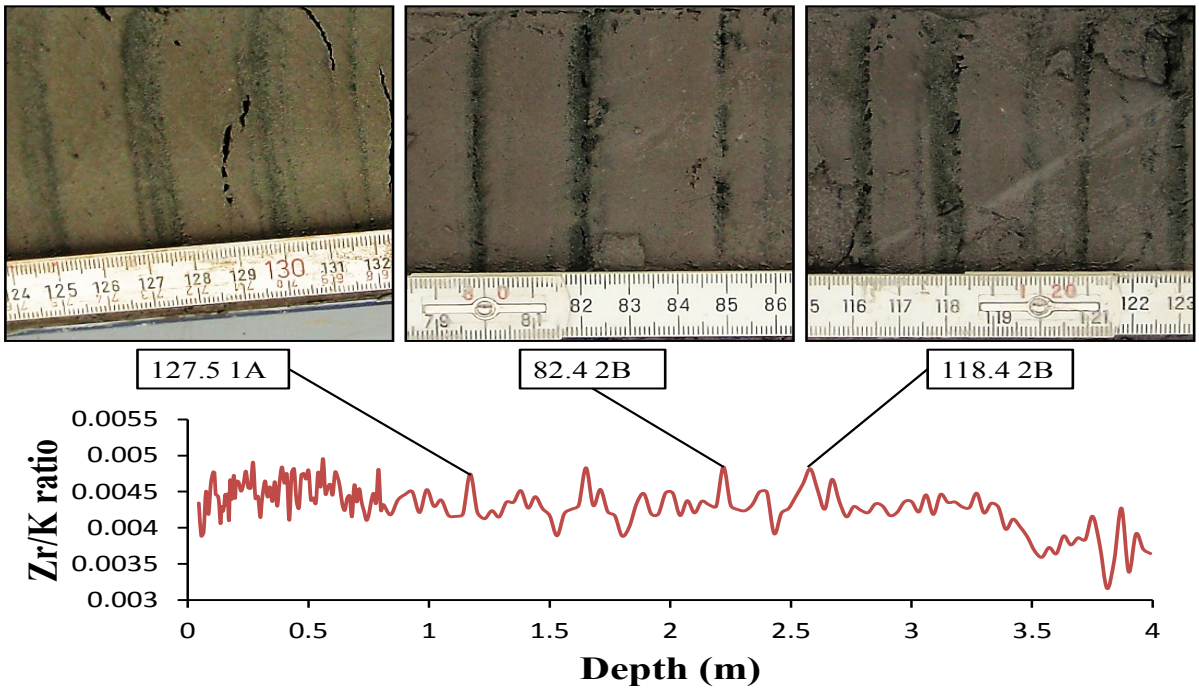

Figure 22. Plot over the Zr/K ratio where increasing values are consistent with increasing minerogenic grain size. The three above pictures denote prominent black layering consistent with increases in the ratio.

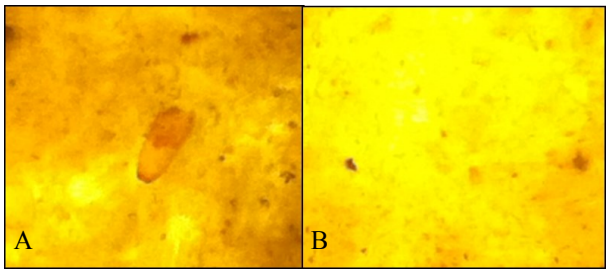

Figure 23. 40x magnification of sediments from A) the general clay gyttja of unit III and B) black banding. The pictures represent the general appearance of the two. In the center of picture A, a typical macrofossil is shown.

interval 8000-4200 cal yrs BP in Lake Storsjön. However, this period does not exhibit an intensified black banding relative to other climatic periods. The lack of response in the mineral magnetic record also rejects the theory of ironsulfide formation at the levels of the black banding, at least the ferromagnetic component. However, if ironsulphide formation was indeed to be present at these levels, a paramagnetic mineral formation such as pyrite would explain the unaltered mineral magnetic record. Pyrite can form diagenetically over the whole range of the pH scale but in Lake Storsjön, which can be assumed have remained rather neutral in pH, pyrite formation would require reducing conditions (Butler 1998). It is here theorized that the black banding do indeed correspond to events of low oxygen conditions and pyritization of fossil magnetite magnetosomes at certain levels due to an sudden and increased influx of sediment causing a reduction of oxygen availability as a response to initially raised oxygen levels and subsequent organic primary production and influx detrital carbon leading to increased bacterial respiration and oxygen consumption. These events may in turn have been initiated by stronger than usual spring meltwater pulses as indicated by the coarsening of the clastic component. No apparent intensification of banding during any interval of the sediment sequence can however be discerned and can thus not be used as a proxy for intensification/reduction of climatic conditions necessary for the induction of such events.

4.5 Recent sedimentary record

The freeze core represents the past 1311 cal yrs BP and is characterized by a highly variable sedimentation rate during the past 800 years, increasing minerogenic concentrations and a slight fining upwards as represented by the lithogenic ratios (Fig. 24). The LOI is also highly variable throughout the freeze core, although a trend to increasing organic content can be discerned in the topmost sediments. Also, the Mn/Fe ratio increases towards the top of the core together with S and Ca concentrations. The inferred oxygenation from the Mn/Fe ratio is in apparent covariance with the LOI (Fig. 8). This contradicts the expected behavior, that increases in organic content would increase microbial respiration, hence consuming oxygen. Koinig et al. (2003) found a similar pattern in a Swiss hard water lake where Mn/Fe ratio started to follow the trend of the LOI from around mid sequence and to the surface. They attributed this behaviour to increased respiration producing more CO_2, subsequently lower-

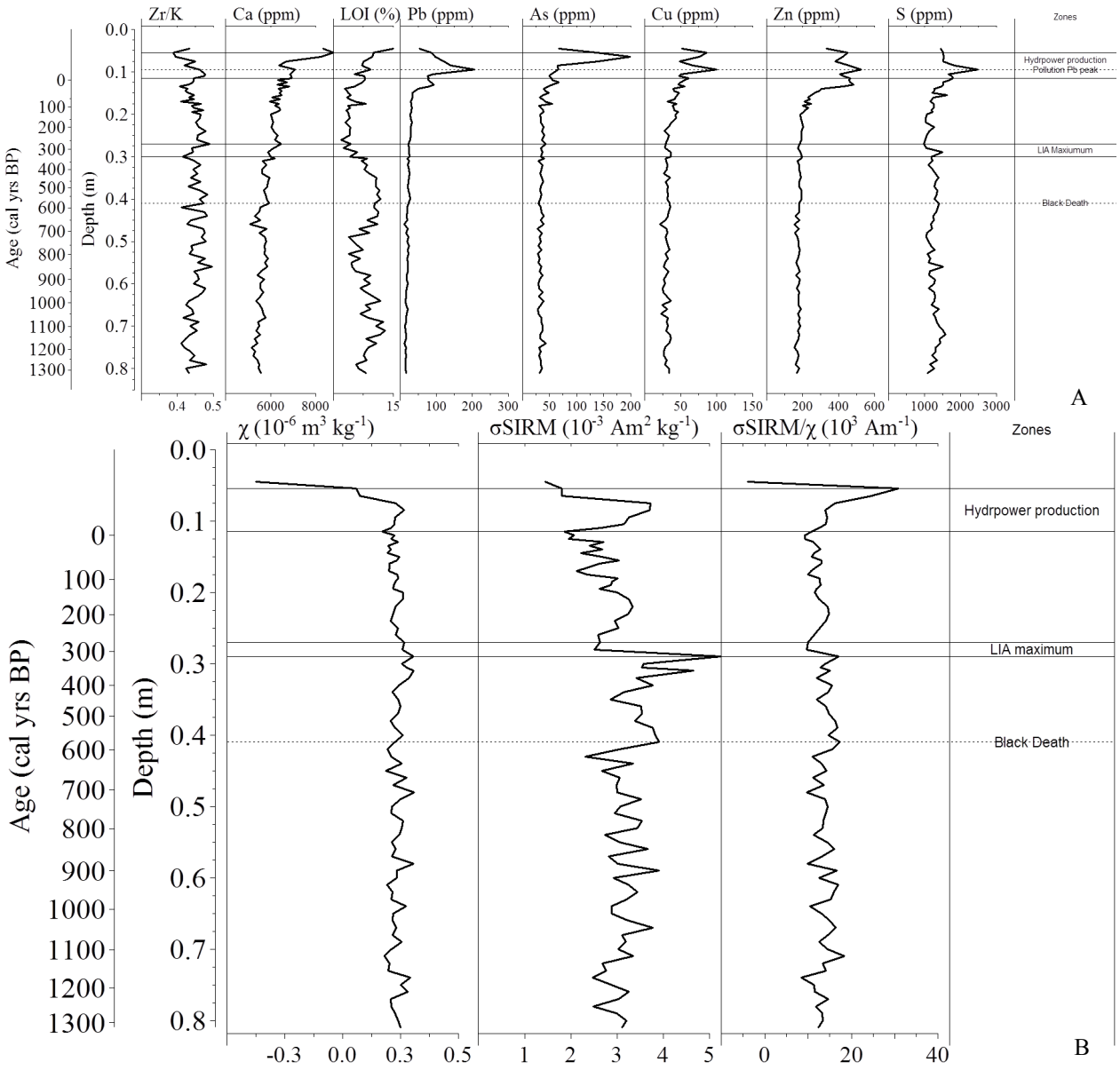

Figure 24. Zoomed up elemental concentrations (A) and mineral magnetic parameters (B) of the freeze core. Zones indicate prominent changes in the records and the corresponding climatic and anthropogenic causes. The upper dashed line in A indicate pollution Pb peak values, but do also correlate with peak concentrations of Cu, Zn and S.

ing the pH. The lowered pH freed Mn from its carbonate bond ($MnCO_3$) and induced the observed bias in the proxy. This behaviour is also applicable to the sediments of Lake Storsjön due to the surrounding carbonaceous bedrock and soils (Fig. 2). In Lake Storsjön the Mn/Fe ratio is beginning to follow the LOI behaviour since around 2800 cal yrs BP, concurrent with the stabilization of the LOI around 13 % (Fig. 24). It is here hypothesized that the Mn/Fe ratio is reflecting past redox conditions up to 2800 cal yrs BP where after the proxy becomes unreliable, but could possibly reflect changes in bottom water pH.

The presence of man in the Lake Storsjön area dates back to around 7000 cal yrs BP. However, it came to have a permanent and considerable population not until around 1000 cal yrs BP (Hemmendorff 1989a). The villages around Lake Storsjön had no major agricultural influence on the land until as late as around 300 cal yrs BP (Hemmendorff 1989b). The existing agricultural land use however, took a hard turn when the Black Death reached Jämtland around AD 1350 (~600 cal yrs BP). This can possibly be discerned as an increase in LOI, decrease in the Zr/K ratio and increase in the σSIRM/χ ratio. This would indicate that the surrounding farmlands in the catchment experienced regrowth as the population tending to the farms decreased. Hence, decreasing the grain size and magnetic grain size of the allochthonous material (Thompson & Edwards 1982, Cuven et al. 2010) to the lake as seen in the sediment record (Fig. 24). The desertion of farmlands around this time (AD 1350) is also highlighted by Abel (1966) and Antonsson (2009)

which corresponds well with the observed changes in the Lake Storsjön sediments.

Between 330-270 cal yrs BP a large change in the LOI, Zr/K ratio, σSIRM, σSIRM/χ ratio and sedimentation rate is apparent. The LOI, sedimentation rate and the mineral magnetic parameters decrease while the Zr/K ratio increase (Fig. 24). The observed changes do not correspond to any significant socioeconomic crisis (ongoing war during "Stormaktstiden" but relatively peaceful in Jämtland) in the area and time. However, the decreasing LOI and sedimentation rate may indicate less favourable conditions for within lake primary production and land use in the catchment area, respectively. The coarsening of allochthonous mineral and mineral magnetic grains as inferred from the Zr/K and σSIRM/χ ratios, respectively, are also consistent with a increased catchment runoff (Zolitschka & Enters 2009), likely as a response to more severe spring meltwater pulses. As to why the σSIRM and χ are decreasing during such events might be related to the composition of the surrounding carbonate rich bedrock, being poor in magnetic minerals. The timing of the observed changes within the sediments are in good agreement with the climatic deterioration of the little ice age (LIA) (see Mathews & Briffa 2005). It has been shown by Briffa et al. (2001) that the northern hemisphere climate was significantly deteriorated, especially during the seventeenth century. This caused abandonment of farmlands similar to that of the Black Death times, described by Neumann and Lindgrén (1979) as the great Estonian famine, which cause (climatic deterioration) also caused famine in Sweden. This famine in contrast to the Black Death was derived from the cooler climate at the time. It is here theorized that the climatic events of the LIA caused the famine experienced in Sweden and the Baltic countries, also including the area around Lake Storsjön. Obviously, the LIA in the area was not limited to a 60 year time window, but seems to have had the most severe impact on agrarian land use during this interval.

After these events, the mineral magnetic parameters decrease upward until around AD 1940 where after a large increase in the mineral magnetic assemblage emerges. The decrease in the mineral magnetic parameters, prior to the 1940^{s}, is accompanied by a quite stable LOI and sedimentation rate (although remarkably low) and does most probably reflect a recovery of agrarian practice and regeneration of vegetation cover. The end of the famine of the seventeenth century represents a time of development. Now the first traces of heavy metal pollution (except for Pb) becomes apparent when examining the early rise in Cu concentrations in the beginning of the eighteenth century (0.26 m depth). Cu is accompanied by rising concentrations of Zn at around early nineteenth century, and lastly As in the late nineteenth century (Fig. 24). This heavy metal pollution succession is interpreted as the onset of the industrial revolution. With growing industry large amounts of trace metals were emitted to the atmosphere and deposited with precipitation and dust (Ross & Granat 1985). The earlier rise in Cu concentrations can probably be attributed to early mining, either local or from a distant source. The Pb concentration starts to increase above background concentrations already around the 12th century (0.75 m) and increases up till AD 1975 when concentrations culminate. The pollution Pb peaks at AD 1200, AD 1530 and AD 1975 (Fig. 9) are clearly reliable since they correlate well with pollution Pb records from sites both north and south of Lake Storsjön (data from Brännvall et al. 1999 & Bindler et al. 2009, Fig. 1). The early Medieval peaks are attributed intensified metallurgy in mainland Europe and Great Britain according to the authors. The recent peak in pollution Pb is related to the intense use of leaded petrol and the subsequent decline represents the ban of such combustible (Renberg 1994).

As previously mentioned, Lake Storsjön is since AD 1938 a regulated reservoir for hydropower production. As seen on water level fluctuation data on decadal mean resolution from Vattenregleringsföretagen (2014) there is a significant rise in the decadal mean lake level when the hydropower production began (Fig. 25). The early 1940^{s} is found, according to the age model, around 0.115 m depth in the sequence. At this depth there are some significant changes in the sediment record. The most pronounced is the exceedingly large rise in sedimentation rate starting at 0.11 m depth. Other changes include increasing values of χ, σSIRM and σSIRM/χ as well as LOI and Ca concentrations. The elevated lake level due to hydropower regulation is in other words seen as an increasing catchment erosion of both clastic and organic material. The consequences of the increased input and sediment sedimentation rate can however not yet be seen. One might expect, learning from previous environmental history of Lake Storsjön, that the large increase in organic matter during a short period of time might cause deteriorated oxygenation of the sediments. The impact of the hydropower regulation on the lake needs to be complemented with an ultra high resolutions study to properly resolve the ongoing change.

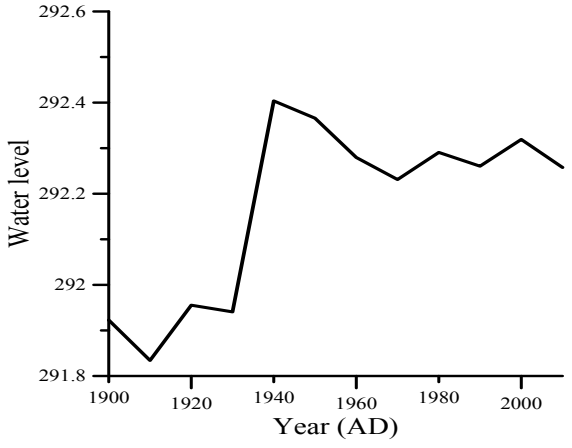

Figure 25. Decadal mean change in water level of Lake Storsjön. Note the large increase in AD 1938 when the hydropower plant was established

5 Final remarks and conclusions

During the work of this thesis, as much as have been learned, as many questions have arisen. The sediment sequence and its characteristics is in many ways indicative of both environmental, climatic and anthropogenic change. However one cannot help to wonder which of the conclusions drawn by the investigations that would be corroborated by another sediment sequence from within the same lake basin. This is of vital importance to bear in top of mind when interpreting geochemical and palaeomagnetic changes from a single sequence in terms of large scale events such as climate change. Hence, the below presented conclusions should be considered as the best effort interpretations of events in need of validation, preferably by additional analysis of at least a second sediment sequence from within the same lake basin. The thesis and its results are indeed the first draft of the description of the Holocene development in Lake Storsjön, Jämtland.

- Relative dating with pollution Pb + PSV proved useful in constructing an age model. The model was in good agreement with external controls (radiocaesium & radiocarbon dating). When the radiocaesium and radiocarbon dates were inserted in the age model, logical assumptions of the sedimentation rates were confirmed and the relative age model strengthened. The deglaciation of the area is believed to have occurred at around 10 000 cal yrs BP, while stagnant ice bodies persisted for an additional 400 years. Thus the drainage of the last ice-lake stage was dated to have occurred around 9 600 cal yrs BP.

- During the Holocene development of Lake Storsjön, changes from high to low oxygen levels in the bottom waters have induced biological, geochemical and magnetic changes to the sediments. Most pronounced are the changes in the Mo/Al ratios, coupled with S concentration increases which are related to increased oxygen consumption as a response to increasing organic sedimentation and/or persisting suboxic to anoxic conditions. The low oxygen conditions favoured sulfide reducing bacteria of which magnetotactic bacteria are an important group. The high coercivity magnetosomes left behind during the events of glacial lake drainage and the 8.2 kyr cooling event by the magnetotactic bacteria is interpreted to be ferromagnetic authigenic greigite.

- Oxygen levels have generally increased since the glacial retreat as inferred from elemental ratios of Mn/Fe. The ratio becomes unreliable above 2800 cal yrs BP as it becomes unexpectedly covariant with concentrations of organic matter. Above 2800 cal yrs BP the Mn/Fe ratio is believed to reflect changes in bottom water pH.

- Anthropogenic impact on Lake Storsjön have been minor. Likely, the population in the area has not been sufficient in historical times to have had any major environmental effect on the lake. However, traces of hardship of the inhabitants of the region can be discerned in the sediment record as changes in catchment erosion and can be linked to both disease and climate change. Furthermore, like most of the Scandinavian lake, Lake Storsjön has suffered the consequences of industrial expansion with the heavy metal pollution that comes with it. Further studies are also needed to resolve the ongoing change caused by hydropower regulations on the lake.

6 Acknowledgements

During the work of this thesis many people have contributed with their time and effort. Special thanks are given to my supervisor Dan Hammarlund for his sound reasoning, encouragement and constant availability. Furthermore, Edouard Regnier is given thanks for his tireless efforts in the field and Ulrich von Grafenstein for his teaching in fieldwork methods and patience with my incompetence (paid penance in full). In the lab, special thanks is directed to Bryan Lougheed for his guiding in the palaeomagnetic field and to Ian Snowball for the recognition and initiation of the long and frightening journey along the palaeomagnetic trail. Furthermore, Inga Labuhn is given thanks for her companionship and spitballing during the laboratory process. I am also forever grateful to Artemis Charalampopoulou, Michelle Karlsson and Emma Fältström for their roughneck efforts in the freeze box during subsampling of the freeze cores. Additionally, Hans Eriksson is thanked for his enthusiastic cooperation in various specialized constructions and in lending out tools and equipment. In the end I also want to thank Richard Bindler, Christer Rönngren and Andreas Nilsson for providing me with reference data.

7 References

Abel, W. 1966. Translated by Ordish, O. 1980: Agricultural fluctuations in Europe from the thirteenth to the twentieth centuries. Methuen and St. Martin´s press. Book review. 363 pp.

Allen, J.R.L. 1999: Geological impacts on coastal wetland landscapes: some general effects of sediment autocompaction in the Holocene of northwestern Europe. *The Holocene 9(1)*, 1-12.

Alley, R.B., Mayewski, P.A., Sowers, T., Stuvier, M., Taylor, K.C. & Clarc, P.U., 1997: Holocene

climate instability: a prominent widespread event 8200 yr ago. *Geology 25*, 483-486.

Antonsson, H. 2009: The extent of farm desertion in central Sweden during the late medieval agrarian crisis: landscape as a source. *Journal of historical geography 35*, 619-641.

Appleby, P.G. 2001: Chronostratigraphic techniques in recent sediments. *In* Last, W.M. & Smol, J.P. (eds.): *Tracking environmental change using lake sediments. Volume 1: Basin analysis, coring and chronological techniques.* Kluwer academic publishers, Dordrecht, pp 171-203.

Axenrot, T., Andersson, M. & Degerman, E., 2013: Fisksammhället I Storsjön, Jämtland. Undersökningar med ekolodning, trålning och nätprovfiske år 2011. Swedish University of agricultural sciences, institution for aquatic resources. *Aqua reports 2013 (6)*.

Battarbee, R.W., Grytnes, J-A., Thompson, R., Appleby, P.G., Catalan, J., Korhola, A., Birks, H.J.B., Heegard, E. & Lami, A., 2002: Comparing palaeolimnological and instrumental evidence of climate change for remote mountain lakes over the last 200 years. *Journal of paleolimnology 28*, 161-179.

Bazylinski, D.A. 1996: Controlled biomineralization of magnetic minerals by magnetotactic bacteria. *Chemical Geology 132*, 191-198.

Benoit, G. & Rozan, T.F. 2001: ^{210}Pb and ^{137}Cs dating methods in lakes: a retrospective study. *Journal of paleolimnology 25*, 455-465.

Bergman, J., Hammarlund, D., Hannon, G., Barnekow, L. & Wohlfarth, B., 2004: Deglacial vegetation succession and Holocene tree-limit dynamics in the Scandes Mountains, west-central Sweden: stratigraphic data compared to megafossil evidence. *Review of palaeobotany and palynology 134*, 129-151.

Bindler, R., Renberg, I., Rydberg, J. & Andrén, T. 2009; Widespread pollution in central Swedish lakes and the Baltic Sea from pre-industrial mining and metallurgy. *Environmental pollution 157*, 2132-2141.

Bjune, A.E., Bakke, J., Nesje, A. & Birks, H.J.B., 2005: Holocene mean July temperature and winter precipitation in western Norway inferred from palynological and glaciological lake-sediment proxies. *The Holocene 15*, 177-189.

Blaauw, M. & Christen, J.A., 2011: Flexible paleoclimate age-depth models using an autoregressive gamma process. *Bayesian analysis 6(3)*, 457-474.

Boës, X. & Renberg, I., 2011: Evaluation of conservative lithogenic elements (Ti, Zr, Al and Rb) to study anthropogenic element enrichments in lake sediments. *Journal of paleolimnology 46*, 75-87.

Bowman, S. 1990: Radiocarbon dating, Interpreting the past. University of California press. 64pp.

Boyle, J.F., 1998: Rapid elemental analysis of sediment samples by isotope source XRF. *Journal of paleolimnology 23*, 213-221.

Brenner, M., Schelske, C.L. & Kenney, W.F. 2004: Inputs of dissolved and particulate ^{226}Ra to lakes and implications for ^{210}Pb dating recent sediments. *Journal of paleolimnology 32*, 53-66.

Briffa, K.R., Osborn, T.J., Schweingruber, F.H., Harris, I.C., Jones, P.D., Shiyatov, S.G. & Vaganov, E.A. 2001: Low-frequency temperature variations from a northern tree ring density network. *Journal of geophysical research 106*, 2929-2941.

Bronks Ramsey, C., 2009: Bayesian analysis of radiocarbon dates. *Radiocarbon, 51(1)*, 337-360.

Brännvall, M.J., Bindler, R., Emteryd, O. & Renberg, I. 2001: Four thousand years of atmospheric pollution in northern Europe: a summary from Swedish sediments. *Journal f paleolimnology 25*, 421-435.

Butler, R.F., 1992: Paleomagnetism: Magnetic domains to geologic terranes. Oxford, Blackwell science, 336 pp.

Christen, J.A. & Fox, C., 2010: A general purpose sampling algorithm for continuous distributions (the t-walk). *Bayesian analysis 4 (2)*, 263-282.

Cohen, S.A., 2003: Paleolimnology, The history and evolution of lake systems. Oxford University Press. 500 pp.

Cuven, S., Francus, P. & Lamoureux, S.F. 2010: Estimation of grain size variability with micro X-ray fluorescence in laminated lacustrine sediments, Cape Bounty, Canadian high arctic. *Journal of Paleolimnology 44*, 803-817.

Dankers, P. 1981: Relationship between median destructive field and remanent coercive forces for dispersed natural magnetite, titanomagnetite and hematite. *Geophysical journal of the Royal Astronomical Society 64*, 447-461.

Davis, B.A.S., Brewer, S., Stevenson, A.C., Guiot, J. & Data contributors., 2003: The temperature of Europe during the Holocene reconstructed from pollen data. *Quaternary science reviews 22*, 1701-1716.

Dean, W.E., Piper, D.Z. & Peterson, L.C. 1999: Mo-

lybdenum accumulation in Cariaco basin sediment over the past 24 ky.: A record of water-column anoxia and climate. *Geology 27 (6)*, 507-510.

Dearing, J., 1994: Environmental magnetic susceptibility, using the Bartington MS2 system. *British library cataloguing in publication data*. 54 pp.

Engstrom, D.R., Swain, E.B. & Kingston, J.C., 1985: A palaeolimnological record of human disturbance from Harvey's Lake, Vermont: geochemistry, pigments and diatoms. *Freshwater biology15*, 261-288.

Eronen, M., Hyvärinen, H. & Zetterberg, P., 1999: Holocene humidity changes in northern Finnish Lapland inferred from lakes sediments and submerged Scots pines dated by tree-rings. *The Holocene 9*, 569-580.

Evans, M.E. & Heller, F. 2003: Environmental magnetism: Principles and applications of enviromagnetics. Elsevier science (USA), 303 pp.

von Grafenstein, U., Erlenkeuser, H., Brauer, A., Jouzel, J. & Johnsen, S.J., 1999: A mid-European decadal isotope-climate record from 15,500 to 5000 years B.P. *Science 284*, 1654-1657.

Hammarlund, D., Björck, S., Buchardt, B., Israelson, C. & Thomsen, C., 2003: Rapid hydrological changes during the Holocene revealed by stable isotope records of lacustrine carbonates from Lake Igelsjön, southern Sweden. *Quaternary science reviews 22*, 353-370.

Hammarlund, D., Velle, G., Wolfe, B.B., Edwards, T.W.D., Barnekow, L., Bergman, J., Holmgren, S., Lamme, S., Snowball, I., Wohlfarth, B. & Possnert, G., 2004: Palaeolimnological and sedimentary responses to Holocene forest retreat in the Scandes Mountains, west-central Sweden. *The Holocene 14*, 862-876.

Heiri, O., Lotter, A.F. & Lemcke, G. 2001: Loss on ignition as a method for estimating organic and carbonate content in sediments: reproducibility and comparability of results. *Journal of paleolimnology 25*, 101-110.

Hemmendorff, O., 1989a: Arkeologi I fjäll skog och bygd. 1 Stenålder – Tidig järnålder. Jämtlands läns museums förlag. 176 pp.

Hemmendorff, O., 1989b: Arkeologi I fjäll skog och bygd. 2 Järnålder - medeltid. Jämtlands läns museums förlag. 176 pp.

Jessen, C.A., Rundgren, M., Björck, S. & Hammarlund, D., 2005: Abrupt climatic changes and an unstable transition into a late Holocene Thermal Decline: a multiproxy lacustrine record from southern Sweden. *Journal of Quaternary science 20(4)*, 349-362.

Johnsen, T.F., Fabel, D. & Stroeven, A.P. 2010: High-elevation cosmogenic nuclide dating of the last deglaciation in the central Swedish mountains: implications for the timing of tree establishment. *Dissertations from the Department of Physical Geography and Quaternary Geology 22*, 1-18.

Kirschvink, J.L. 1980: The least-squares line and plane and the analysis of palaeomagnetic data. *Geophysical Journal International 62(3)*, 699-718.

Klaminder, J., Appleby, P., Crook, P. & renberg, I. 2012: Post-deposition diffusion of 137Cs in lake sediments: Implications for radiocaesium dating. *Sedimentology 59*, 2259-2267.

Koinig, K.A., Shotyk, W., Lotter, A.F., Ohlendorf, C. & Sturm, M. 2003: 9000 years of geochemical evolution of lithogenic major and trace elements in the sediment of an alpine lake – the role of climate, vegetation, and land-use history. *Journal of paleolimnology 30*, 307-320.

Lundqvist, J. 1973: Isavsmältningens förlopp I Jämtlands län. *Sveriges geologiska undersökning, avhandlingar och uppsattser 66 (12)*, 187 pp.

Lundqvist, J. 2009: Weichsel-istidens huvudfas. *In* C. Fredén (ed): *Berg och jord, tredje utgåvan*. Sveriges nationalatlas redaktion. 208 pp.

Lyons, T.W., Werne, J.P., Hollander, D.J. & Murray, R.W. 2003: Contrasting sulfur geochemistry and Fe/Al and Mo/Al ratios across the last oxic-to-anoxic transition in the Cariaco Basin, Venezuela. *Chemical Geology 195*, 131-157.

Magny, M., Bégeot, C., Guiot, J. &Peyron, O., 2003: Contrasting patterns of hydrological changes in Europe in response to Holocene climatic cooling phases. *Quaternary science reviews 22*, 1589-1596.

Matthews, J.A. & Briffa, K. 2005: The 'Little Ice Age': Re-evaluation of an evolving concept. *Geografiska annaler 87(A)*, 17-36.

Moskowitz, B.M. 1991. Hitchhiker's guide to magnetism. Environmental magnetism workshop 5-8 June, 1991. Institute of rock magnetism, University of Minnesota.

Naeher, S., Gilli, A., north, R.P., Hamann, Y. & Schubert, C.J. 2013: Tracing bottom water oxygenation with sedimentary Mn/Fe ratios in Lake Zurich, Switzerland. *Chemical Geology 352*, 125-133.

Nesje, A., Matthews, J.A., Dahl, S.O., Berrisford, M.S.

& Andersson, C., 2001: Holocene glacier fluctuations of Flatebreen and winter precipitation changes in the Jostedalsbreen region, western Norway, based on glaciolacustrine sediment records. *The Holocene 11*, 267-280.

Neumann, J. & Lindgrén, S. 1979: Great historical events that were significantly affected by the wather: 4, the great famines in Finland and Estonia, 1695-97. *Bulletin of the American meterological society 60*, 775-787.

Odegaard, C., Rea, D.K. & Moore Jr, T.C. 2003: Stratigraphy of the mid-Holocene black bands in Huron: Evidence for possible basin-wide anoxia. *Journal of paleolimnology 29*, 221-234.

Oswald, W.W., Anderson, P.M., Brown, T.A., Brubaker, L.B., Hu, F.S., Lozhkin, A.V., Tinner, W. & Kaltenrieder, P. 2003: Effects of sample mass and macrofossil type on radiocarbon dating of arctic and boreal lake sediments. *The Holocene 15(5)*, 758-767.

Petterson, G., Renberg, I., Sjöstedt-de luna, S., Arnqvist, P. & Anderson, N.J., 2010: Climatic influence on the inter-annual variability of late-Holocene minerogenic sediment supply in a boreal forest catchment. *Earth surface processes and landforms 35*, 390-398.

Piper, D.Z & Isaacs, C.M. 1995: Geochemistry of minor elements in the Monterey formation, California: seawater chemistry of deposition. *U.S. Geological survey professional paper 1556*, 1-46.

Reimer, P.J., Bard, E., Bayliss, A., Beck, J.W., Blackwell, P.G., Bronk Ramsey, C., Buck, C.E., Edwards, R.L., Friedrich, M., Grootes, P.M., Guilderson, T.P., Haflidason, H., Hajdas, I., Hatté, C., Heaton, T.J., Hoffmann, D.L., Hogg, A.G., Hughen, K.A., Kaiser, K.F., Kromer, B., Manning, S.W., Niu, M., Reimer, R.W., Richards, D.A., Scott, M.E., Southon, J.R., Turney, C.S.M. & van der Plicht, J. 2013: IntCal13 and Marine13 radiocarbon age calibration curves 0-50,000 yr cal BP. *Radiocarbon 55(4)*, 1869-1887.

Reinholdsson, M., Snowball, I., Zillén, L., Lenz, C. & Conley, D.J. 2013: Magnetic enhancement of Baltic Sea sapropels by greigite magnetofossils. *Earth and planetary science letters 366*, 137-150.

Renberg, I. & Hansson, H. 1993: A pump freeze corer for recent sediments. *Limnology and oceanography 38(6)*, 1317-1321.

Renberg, I., Wik Persson, M. & Emteryd, O. 1994: Pre-industrial atmospheric lead contamination detected in Swedish lake sediments. *Nature 368*, 323-326.

Renssen, H., Seppä, H., Heiri, O., Roche, D.M., Goosse, H. & Fichefet, T., 2009: The spatial and temporal complexity of the Holocene thermal maximum. *Nature geoscience letters 2*, 411-414.

Ross, H.B. & Granat, L. 1985: Deposition of atmospheric trace metals as measured in the snowpacks. *Tellus 38B*, 27-43.

Seppä, H. & Birks, H.J.B., 2000: July mean temperature and annual precipitation trends during the Holocene in Fennoscandian tree-line area: pollen-based climate reconstructions. *The Holocene 11*, 527-539.

Smol, P.J., 2008: Pollution of lakes and rivers: A paleoenvironmental perspective, 2nd edition. Wiley-Blackwell. 396 pp.

Snowball, I.F., 1994: Bacterial magnetite and magnetic properties of sediments in a Swedish lake. *Earth and planetary science letters 126*, 12-142.

Snowball, I., Zillén, L., Ojala, A., Saarinen, T. & Sandgren, P. 2007: FENNOSTACK and FENNORPIS: varve dated Holocene palaeomagnetic secular variation and relative palaeointensity stacks for Fennoscandia. *Earth and planetary science letters 255*, 106-116.

Snowball, I., Zillén, L. & Sandgren, P. 2002: Bacterial magnetite in swedish varved lake sediments: a potential bio-marker of environmental change. *Quaternary International 88*, 13-19.

Stanton, T., Snowball, I., Zillén, L. & Wastegård, S. 2010: Validating a Swedish varave chronology using radiocarbon, palaeomagnetic secular variation, lead pollution and statistical correlation. *Quaternary geochronology 5*, 611-624.

Taboada, T., Martinez Cortizas, A., García, C. & García-Rodeja, E. 2005: Particle-size fractionation of titanium and zirconium during weathering and pedogenesis of granitic rocks in NW Spain. *Geoderma 131*, 218-236.

Thompson, R. & Edwards, K.J. 1982: A Holocene palaeomagnetic record and geomagnetic master curve from Ireland. *Boreas 11*, 335-349.

Thompson, R. & Oldfield, F. 1986: Environmental magnetism. Allen & Unwin Ltd, 227 pp.

Weiss, D., Shotyk, W., Appleby, P.G., Kramers, J.D. & Cheburkin, A.K. 1999: Atmospheric Pb deposition since the industrial revolution recorded by five Swiss peat profiles: Enrichment factors, fluxes isotopic composition, and sources. *Environmental science and technology 33*, 1340-

1352.
Zijderveld, J.D.A. 1967: AC demagnetization of rocks: analysis of results. *In* D.W. Collinson, K.M. Creer & S.K. Runcorn (eds): *Methods in Paleomagnetism*, 254-286.
Zolitschka, B. 2007: Varved lake sediments. *In* S.A. Elias (ed.): *Encyclopedia of Quaternary Science.* Elsevier, Amsterdams, 3105-3114 pp.
Zolitschka, B. & Enters, D., 2009: Lacustrine sediments. *In* V. Gornitz (ed.): *Encyclopedia of paleoclimatology and ancient environments.* Springer Science+Business Media B.V, 1048 pp.

Tidigare skrifter i serien "Examensarbeten i Geologi vid Lunds universitet":

375. Grenholm, Mikael, 2014: The Birimian event in the Baoulé Mossi domain (West African Craton) — regional and global context. (45 hp)
376. Hafnadóttir, Marín Ósk, 2014: Understanding igneous processes through zircon trace element systematics: prospects and pitfalls. (45 hp)
377. Jönsson, Cecilia A. M., 2014: Geophysical ground surveys of the Matchless Amphibolite Belt in Namibia. (45 hp)
378. Åkesson, Sofia, 2014: Skjutbanors påverkan på mark och miljö. (15 hp)
379. Härling, Jesper, 2014: Food partitioning and dietary habits of mosasaurs (Reptilia, Mosasauridae) from the Campanian (Upper Cretaceous) of the Kristianstad Basin, southern Sweden. (45 hp)
380. Kristensson, Johan, 2014: Ordovicium i Fågelsångskärnan-2, Skåne – stratigrafi och faciesvariationer. (15 hp)
381. Höglund, Ida, 2014: Hiatus - Sveriges första sällskapsspel i sedimentologi. (15 hp)
382. Malmer, Edit, 2014: Vulkanism - en fara för vår hälsa? (15 hp)
383. Stamsnijder, Joaen, 2014: Bestämning av kvartshalt i sandprov - metodutveckling med OSL-, SEM– och EDS-analys. (15 hp)
384. Helmfrid, Annelie, 2014: Konceptuell modell över spridningsvägar för glasbruksföroreningar i Rejmyre samhälle. (15 hp)
385. Adolfsson, Max, 2014: Visualizing the volcanic history of the Kaapvaal Craton using ArcGIS. (15 hp)
386. Hajny, Casandra, 2014: Ett mystiskt ryggradsdjursfossil från Åsen och dess koppling till den skånska, krittida ryggradsdjursfaunan. (15 hp)
387. Ekström, Elin, 2014: – Geologins betydelse för geotekniker i Skåne. (15 hp)
388. Thuresson, Emma, 2014: Systematisk sammanställning av större geoenergianläggningar i Sverige. (15 hp)
389. Redmo, Malin, 2014: Paleontologiska och impaktrelaterade studier av ett anomalt lerlager i Schweiz. (15 hp)
390. Artursson, Christopher, 2014: Comparison of radionuclide-based solar reconstructions and sunspot observations the last 2000 years. (15 hp)
391. Svahn, Fredrika, 2014: Traces of impact in crystalline rock – A summary of processes and products of shock metamorphism in crystalline rock with focus on planar deformation features in feldspars. (15 hp)
392. Järvin, Sara, 2014: Studie av faktorer som påverkar skredutbredningen vid Norsälven, Värmland. (15 hp)
393. Åberg, Gisela, 2014: Stratigrafin i Hanöbukten under senaste glaciationen: en studie av borrkärnor från IODP's expedition nr 347. (15 hp)
394. Westlund, Kristian, 2014: Geomorphological evidence for an ongoing transgression on northwestern Svalbard. (15 hp)
395. Rooth, Richard, 2014: Uppföljning av utlastningsgrad vid Dannemora gruva; april 2012 - april 2014. (15 hp)
396. Persson, Daniel, 2014: Miljögeologisk undersökning av deponin vid Getabjär, Sölvesborg. (15 hp)
397. Jennerheim, Jessica, 2014: Undersökning av långsiktiga effekter på mark och grundvatten vid infiltration av lakvatten – fältundersökning och utvärdering av förhållanden vid Kejsarkullens avfallsanläggning, Hultsfred. (15 hp)
398. Särman, Kim, 2014: Utvärdering av befintliga vattenskyddsområden i Sverige. (15 hp)
399. Tuvesson, Henrik, 2014: Från hav till land – en beskrivning av geologin i Skrylle. (15 hp)
400. Nilsson Brunlid, Anette, 2014: Paleoekologisk och kemisk-fysikalisk undersökning av ett avvikande sedimentlager i Barsebäcks mosse, sydvästra Skåne, bil dat för ca 13 000 år sedan. (15 hp)
401. Falkenhaug, Jorunn, 2014: Vattnets kretslopp i området vid Lilla Klåveröd: ett kunskapsprojekt med vatten i fokus. (15 hp)
402. Heingård, Miriam, 2014: Long bone and vertebral microanatomy and osteohistology of 'Platecarpus' ptychodon (Reptilia, Mosasauridae) – implications for marine adaptations. (15 hp)
403. Kall, Christoffer, 2014: Microscopic echinoderm remains from the Darriwilian (Middle Ordovician) of Västergötland, Sweden – faunal composition and applicability as environmental proxies. (15 hp)
404. Preis Bergdahl, Daniel, 2014: Geoenergi

för växthusjordbruk – Möjlig anläggning av värme och kyla i Västskåne. (15 hp)

405. Jakobsson, Mikael, 2014: Geophysical characterization and petrographic analysis of cap and reservoir rocks within the Lund Sandstone in Kyrkheddinge. (15 hp)
406. Björnfors, Oliver, 2014: A comparison of size fractions in faunal assemblages of deep-water benthic foraminifera—A case study from the coast of SW-Africa.. (15 hp)
407. Rådman, Johan, 2014: U-Pb baddeleyite geochronology and geochemistry of the White Mfolozi Dyke Swarm: unravelling the complexities of 2.70-2.66 Ga dyke swarms on the eastern Kaapvaal Craton, South Africa. (45 hp)
408. Andersson, Monica, 2014: Drumliner vid moderna glaciärer — hur vanliga är de? (15 hp)
409. Olsenius, Björn, 2014: Vinderosion, sanddrift och markanvändning på Kristianstadsslätten. (15 hp)
410. Bokhari Friberg, Yasmin, 2014: Oxygen isotopes in corals and their use as proxies for El Niño. (15 hp)
411. Fullerton, Wayne, 2014: REE mineralisation and metasomatic alteration in the Olserum metasediments. (45 hp)
412. Mekhaldi, Florian, 2014: The cosmic-ray events around AD 775 and AD 993 - Assessing their causes and possible effects on climate. (45 hp)
413. Timms Eliasson, Isabelle, 2014: Is it possible to reconstruct local presence of pine on bogs during the Holocene based on pollen data? A study based on surface and stratigraphical samples from three bogs in southern Sweden. (45 hp)
414. Hjulström, Joakim, 2014: Bortforsling av kaxblandat vatten från borrningar via dagvattenledningar: Riskanalys, karaktärisering av kaxvatten och reningsmetoder. (45 hp)
415. Fredrich, Birgit, 2014: Metadolerites as quantitative P-T markers for Sveconorwegian metamorphism, SW Sweden. (45 hp)
416. Alebouyeh Semami, Farnaz, 2014: U-Pb geochronology of the Tsineng dyke swarm and paleomagnetism of the Hartley Basalt, South Africa – evidence for two separate magmatic events at 1.93-1.92 and 1.88-1.84 Ga in the Kalahari craton. (45 hp)
417. Reiche, Sophie, 2014: Ascertaining the lithological boundaries of the Yoldia Sea of the Baltic Sea – a geochemical approach. (45 hp)
418. Mroczek, Robert, 2014: Microscopic shock-metamorphic features in crystalline bedrock: A comparison between shocked and unshocked granite from the Siljan impact structure. (15 hp)
419. Balija, Fisnik, 2014: Radon ett samhällsproblem - En litteraturstudie om geologiskt sammanhang, hälsoeffekter och möjliga lösningar. (15 hp)
420. Andersson, Sandra, 2014: Undersökning av kalciumkarbonatförekomsten i infiltrationsområdet i Sydvattens vattenverk, Vombverket. (15 hp)
421. Martin, Ellinor, 2014: Chrome spinel grains from the Komstad Limestone Formation, Killeröd, southern Sweden: A high-resolution study of an increased meteorite flux in the Middle Ordovician. (45 hp)
422. Gabrielsson, Johan, 2014: A study over Mg/Ca in benthic foraminifera sampled across a large salinity gradient. (45 hp)
423. Ingvaldson, Ola, 2015: Ansvarsutredningar av tre potentiellt förorenade fastigheter i Helsingborgs stad. (15 hp)
424. Robygd, Joakim, 2015: Geochemical and palaeomagnetic characteristics of a Swedish Holocene sediment sequence from Lake Storsjön, Jämtland. (45 hp)

LUNDS UNIVERSITET

Geologiska institutionen

Lunds universitet